GEOLOGY AND GEOCHRONOLOGY OF THE SPIRIT MOUNTAIN BATHOLITH, SOUTHERN NEVADA: IMPLICATIONS FOR TIMESCALES AND PHYSICAL PROCESSES OF BATHOLITH CONSTRUCTION

By

Barry Alan Walker, Jr.

Thesis

Submitted to the Faculty of the

Graduate School of Vanderbilt University

In partial fulfillment of the requirements

for the degree of

MASTER OF SCIENCE

in

Earth and Environmental Sciences

May, 2006

Nashville, Tennessee

Approved

Professor Calvin F. Miller

Professor John C. Ayers

ACKNOWLEDGEMENTS

First and foremost, I would like to thank Dr. Calvin Miller. He's the man. Calvin has been a leader in everything from geology to vocabulary building to good living. I don't think he's ever been a jerk (an aspect of his character I furiously admire and will seek, for the rest of my life, to emulate). Thank you, Calvin, for all your time, energy, and guidance. Others: Dr. Joe Wooden at USGS/Stanford provided invaluable input and guidance throughout the data collection and reduction process. Thanks to Dr. Jonathan Miller at San Jose State University, whose discussions and ideas advanced this project. I thank Dr. John Ayers for reading this thesis with interest and offering helpful suggestions. Dr. Steve Ludington with the USGS in Menlo Park also gave helpful input and turned me onto some interesting imagery. Lily Lowery, a fellow Sewanee graduate, yielded her time and energy in the field, lab, and office. The many discussions I've had with Lily about this project have been fantastic. Ben George, my field assistant for a month, helped me gather data and throw around ideas. Our long, hot days and fireside chats are fond memories of mine. I thank the Department of Earth and Environmental Sciences for the teaching assistantships I held, and all the support the students and faculty have given me. Thanks to the Graduate School for helping to fund my presentation at the American Geophysical Union Joint Assembly, spring 2005. I'd like to thank Lanier, my lady, for always being as supportive as humanly possible, and for giving me nice thought-breaks when geology wasn't looking so nice. And finally, my mother and father for reasons I won't try to get into. Financial support for this project came from NSF grants EAR-0409876 and EAR-0107094.

TABLE OF CONTENTS

Appendices

LIST OF TABLES

LIST OF FIGURES

CHAPTER I

INTRODUCTION

Summary

The Spirit Mountain batholith (SMB) is a ~250 km^2 composite silicic intrusion located within the Colorado River Extensional Corridor (CREC) in southernmost Nevada. Westward tilting of 40-50° has exposed a cross section from the roof through deep levels of the SMB. Piecemeal construction is indicated by zircon geochronology, field relations, and elemental geochemistry. U/Pb data (zircon SHRIMP) demonstrates a ~2 million year (17.4-15.3 Ma) history for the SMB. Individual samples contain zircons with ages that span the lifetime of the batholith, suggesting recycling of extant zircon into new magma pulses. Field relations reveal several distinct magmatic episodes and suggest a common injection geometry of stacked horizontal sheeting.

The largest unit of the SMB is a gradational section (from roof to depth) of high-silica leucogranite through coarse granite into foliated quartz monzonite and has a ~million year history. The 25 km^2 x 2 km^2 leucogranite zone was emplaced incrementally as subhorizontal sheets over most or all of the million year history of this section, suggesting repeated fractional crystallization and melt segregation events. The quartz monzonite is the cumulate residuum of this fractionation. Age data from throughout this gradational unit show multiple zircon populations within individual samples. Subsequent distinct intrusions that cut this large unit, which include minor

populations of zircons corresponding to earlier magmatic events, preserve a sheeted, sill-on-sill geometry.

We envision the SMB to have been a patchwork of melt-rich, melt-poor, and entirely solid zones throughout its active life. Preservation of intrusion geometries and contacts depended on the consistency of the host rock. Zircons recycled into new pulses of magma document remobilization of previously emplaced crystal mush, suggesting the mechanisms by which evidence for initial construction of the batholith became blurred.

Scope

Prevailing views of the nature of magma chambers and pluton construction have been challenged in recent years. Recent geochronological studies of volcanic and plutonic rocks suggest that magmatic *systems* may be long-lived, on the order of $>10^5$ to $>10^6$ years (Halliday et al., 1989; Mahood, 1990; Davies et al., 1994; Brown & Fletcher, 1999; Schmitt et al., 2002; Grunder & Klemetti, 2005; Vazquez & Reid, 2002; Charlier et al., 2005, Miller and Wooden, 2004; Hildreth, 2004; Cates et al., 2003; Hawkins & Wiebe, 2003; Coleman et al., 2004; Cruden et al., 2005; Simon and Reid, 2005; Walker et al., 2005) - longer than the anticipated lifespan of a large magma body as indicated by thermal modelling (Glazner et al., 2004). Evidence has been cited that many exposed plutons are composite, formed by multiple replenishments of both monotonously similar and highly contrasting magma (Wiebe, 1994; Paterson & Miller, 1998; Miller & Miller, 2002; Hawkins and Wiebe, 2004; Glazner et al., 2004), and similar processes have been inferred for chambers that feed volcanoes (Eichelberger et al., 2000; Bacon and Metz, 1984; Koyaguchi and Kaneko, 2000; Hildreth, 1981). The importance, or even the existence, of an identifiable magma chamber in the construction of plutons has been questioned (Glazner et al., 2004), based in part upon the inability of geophysical investigations to identify sizable zones with high melt-rich fraction in the Earth's crust (eg. Iyer et al., 1990; Lees, 2005) as well as on evidence for piecemeal accumulation over protracted periods. And yet giant eruptions provide indisputable evidence that large reservoirs of melt-rich, felsic magma do reside, at least from time to time, beneath the Earth's surface (Hildreth, 1981; Bachmann et al., 2002; Chesner et al., 1991; Christiansen, 1984).

The purpose of this paper is two-fold. The first objective is to describe and interpret the Spirit Mountain batholith, a large composite intrusion that is well exposed in cross-section in southernmost Nevada. The second is to discuss how the magmatic history of this batholith may illuminate issues regarding the timescales and physical processes of accumulation of granitic rock in the upper crust. A combination of U-Pb (SHRIMP zircon) data, field relations, and elemental geochemistry of the batholith reveals a protracted history of repeated replenishment, remobilization, and segregation of fractionated melt. The patchwork character of this intrusion may mark a common process of batholith construction that, in part, reconciles conflicting evidence regarding the existence of large, felsic magma chambers.

CHAPTER II

GEOLOGIC BACKGROUND

Volborth (1973) first mapped and described the "Spirit Mountain block" in the Newberry Mountains of southern Nevada. He identified the Spirit Mountain block as a Tertiary pluton, and generally described its structure and petrology. Subsequent studies (Hopson et al,. 1994; Howard et al., 1994; Faulds et al., 1992) established the Spirit Mountain pluton and the adjacent Mirage pluton as tilted granite complexes. These two plutons have since been considered separate intrusions, but based on chemistry, geochronology, and field relations, we refer to them and other smaller intrusive units collectively as the Spirit Mountain batholith. Preliminary geochronological studies of the Spirit Mountain system yielded ages of 17 Ma (U-Pb in sphene; Howard et al., 1996) and 20 Ma (Rb-Sr whole rock; Ramo et al., 1999). The Mirage pluton yielded an age of 15 Ma (U-Pb in zircon; Howard et al., 1996). Elemental and isotopic studies comparing the Spirit Mountain "pluton" to Proterozoic rapakivi granites show that the Spirit Mountain magmas probably had a feldspar-dominated, relatively hybrid crustal source (Haapala et al., 1995, 1996; Ramo et al., 1999; Haapala et al., 2005).

The Spirit Mountain batholith (SMB) is located within the northern Colorado River Extensional Corridor (CREC) (Figure 1), which experienced crustal thinning and related magmatism in the mid Miocene, from ~16 – 11 Ma (Faulds et al., 1995; Gans and Bohrson, 1998; Howard et al., 1996). The SMB is bounded on the east by the Newberry Mountains detachment fault, a major normal fault that experienced 10-15 km of top-to the-east slip (Faulds et al., 2001). The batholith was tilted 40-50° westward, as indicated by (1) paleomagnetic data (Faulds et al., 1992), (2) west-east progression from miarolitic leucogranite to foliated quartz monzonite within the SMB (Hopson et al., 1994), and (3) east dipping dikes, thought to have intruded vertically (Faulds et al., 1992). This tilting affords a cross section of the batholith in map view, with a westward paleo-up direction.

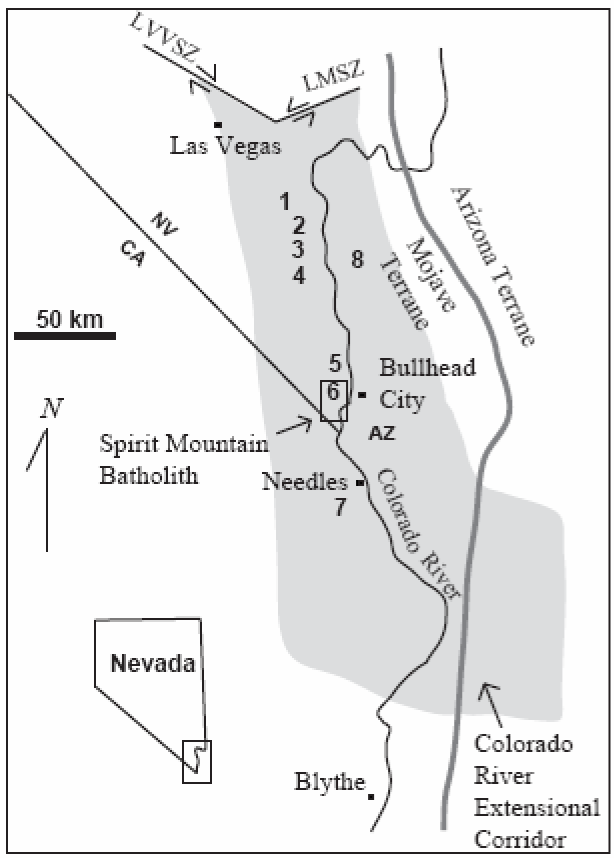

Figure 1: Southernmost Nevada and adjacent California and Arizona with Spirit Mountain batholith and other plutons, the northern Colorado River Extensional Corridor, and the Mojave-Arizona terrane boundary (Bennett and Depaolo, 1987; Wooden and Miller, 1990). Miocene plutons: 1—Boulder City; 2—Nelson; 3—Aztec Wash; 4—Searchlight; 6—Spirit Mountain batholith; 7—Sacramento; 8—Mt. Perkins. 5 is the Cretaceous White Rock Wash pluton. SVVSZ—Las Vegas Valley shear zone; LMSZ—Lake Meade shear zone. Towns shown for reference.

The SMB intruded three extant units: a 1.7 Ga gneiss complex, a 1.4 Ga megacrystic granite, and the Late Cretaceous White Rock Wash Pluton. Protoliths of the 1.7 Ga gneiss include granitic, metasedimentary, and mafic igneous rocks (Volborth, 1973). The 1.4 Ga granite, part of the belt of mid-Proterozoic “anorogenic” plutons that stretches across North America and into northern Eupore (Anderson and Morrison, 2005), is characterized by large (locally >5 cm), euhedral alkali-feldspar crystals within a dark ground mass. Locally, the granite is weakly to strongly mylonitized. The White Rock Wash pluton is a quartz-rich, locally garnet-bearing, two-mica granite, and has yielded ages of ~70 Ma (SHRIMP monazite; Miller et al., 1997) and 65 Ma (Rb-Sr whole rock; Ramo et al., 1999).

Four other Miocene plutons of similar age, all dominantly granitic with small to large mafic components, lie within the northern CREC in the vicinity of SMB: Aztec Wash pluton (15.6-15.8 Ma), Searchlight pluton (17.7-15.8 Ma), Mt. Perkins pluton (15.8-16.0 Ma), and Nelson pluton (~16.5) (Falkner et al., 1995; Metcalf et al., 1995; Faulds et al., 1995; Bachl et al., 2001; Cates et al., 2003, Miller et al., 2004, Lee et al, 1995). The Searchlight pluton, interpreted to have a thick sequence of quartz monzonite cumulate beneath a higher zone of granite, is similar to the SMB (Bachl et al., 2001). The Newberry dike swarm (George et al., 2005), which cuts the SMB, is very similar in petrology and scale to the Eldorado dike swarm that cuts the Searchlight, Aztec Wash, and Nelson plutons (Steinwinder et al., 2004, Bachl et al., 2001; Falkner et al., 1995).

CHAPTER II

METHODS

Thirteen fresh samples were selected for zircon geochronology (see Table 1**)**. Zircons were separated using standard procedures at Vanderbilt University, mounted in epoxy, polished, and imaged by cathodoluminescence (CL) on the JEOL JSM 5600 scanning electron microscope at Stanford University. Spots on the zircons ~30-40 μm in diameter were analyzed using the Stanford/USGS Sensitive High Resolution Ion Microprobe, Reverse Geometry (SHRIMP-RG) at Stanford University. Zircon standards R33 (419 Ma) and CZ3 (550 ppm U, 29.5 ppm Th) at the Stanford/USGS facility were used as U-Pb isotopic and U and Th concentration standards, respectively.

Forty-eight samples were selected for geochemical analysis. Sample locations are located in Appendix B. Whole rock powders were prepared from fresh samples using an alumina ceramic shatter box at Vanderbilt and analyzed for major and trace elements by Activation Laboratories Ltd. (Ontario, Canada), using inductively coupled plasma mass spectrometry and instrumental neuron activation analysis.

CHAPTER IV

LITHOLOGIES AND FIELD RELATIONS

Overview

The Spirit Mountain Batholith is exposed over an area of about ~250 km^2 (Figure 2). Exposure of fresh rock in most of the western (upper) ~7 km of the SMB is almost continuous. Narrow canyons provide good exposures in the eastern portion of the batholith, but outside the canyons, exposure is limited and rocks become increasingly altered toward the Newberry Mountains detachment. Zones of mylonitization, fracturing, and alteration lead us to infer two large ~N-S striking faults in this generally poorly exposed area (see Figure 2), but their continuity and magnitude of displacement remain uncertain. Lithologies permit the interpretation that normal displacement along these faults has resulted in the repetition of a portion of the batholith. Our characterization of this poorly exposed northeastern part of the SMB and of the Mirage granite therefore remain less complete than that of the western part of the batholith.

Much of the well exposed portion of the SMB appears locally homogeneous, but close examination of field relations reveals that it varies subtly throughout, and as a whole it exhibits a wide variety of textures and compositions. With the cross sectional view afforded by tilting, it is apparent that most of this area has a fairly consistent textural and chemical stratigraphy from west to east (top to bottom) that is laterally continuous from north to south (cf. Hopson et al., 1994). This stratigraphy is interrupted

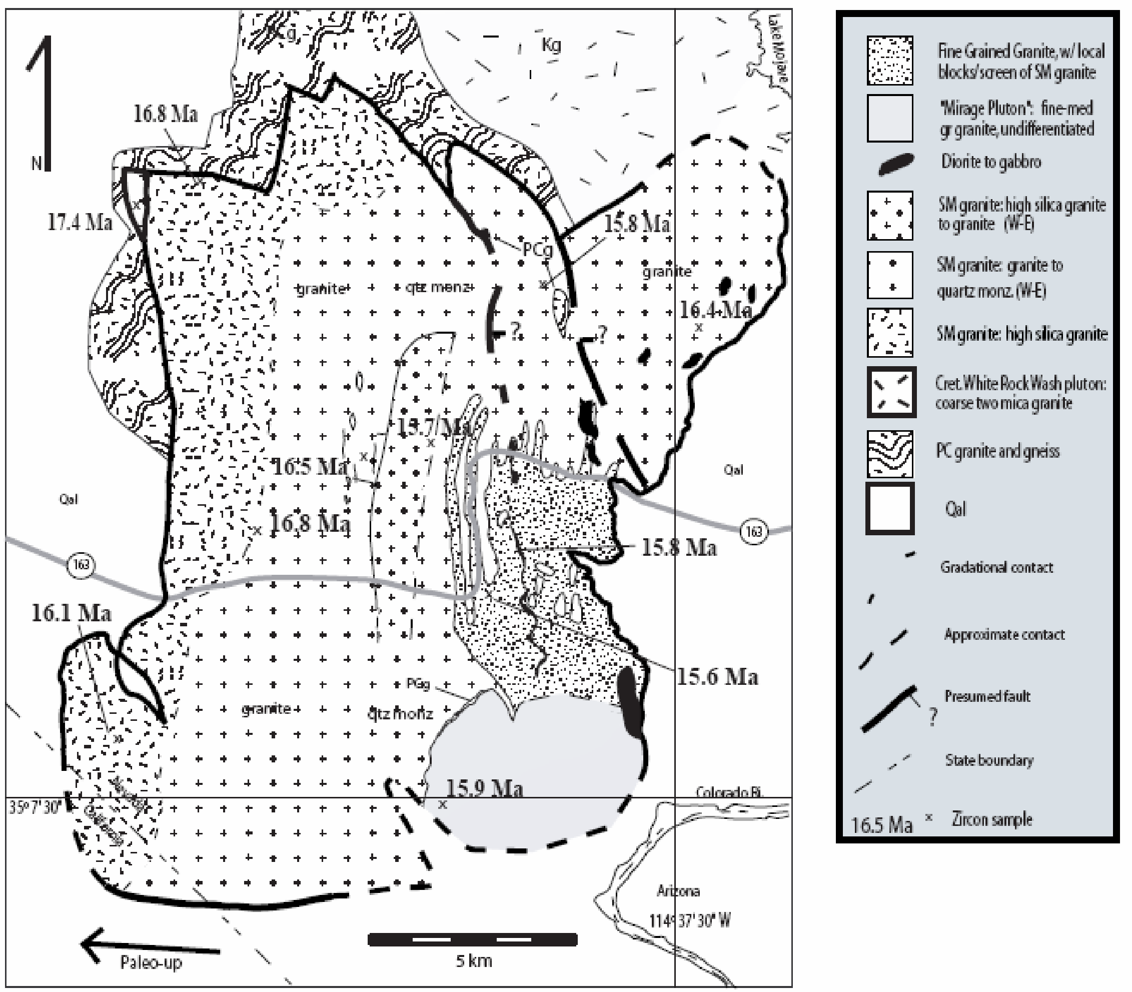

Figure 2: Geologic Map of the Spirit Mountain batholith. Up direction prior to tilting indicated by arrow. Highway 163 shown for reference. Newberry Mountains dike swarm cuts through the central portion of the batholith but is absent to avoid visual complication.

in several places by younger intrusions. The entire SMB, including later intrusions and more poorly exposed sections, consists mostly of granitic rock with identical mineral assemblages. Dioritic to basaltic dikes, sills and pods are present, but they are volumetrically minor in comparison to the granites; the sills and pods are restricted to the lower 1/3 of the batholith, and the dikes are part of the late Newberry swarm that marks termination of the intrusive history.

The granitoids all contain varying proportions of the assemblage plagioclase + alkali feldspar + quartz + biotite + accessories (sphene [titanite], apatite, allanite [and/or chevkinite], zircon, and opaques, fluorite in some leucogranites, and schorl tourmaline in some pegmatites). Accessory minerals are generally euhedral and are enclosed in all other phases. Biotite, plagioclase, and in most cases alkali feldspar are subhedral to euhedral, suggesting that all were early liquidus phases. Quartz is interstitial in less felsic rocks and forms prominent subhedral crystals in more felsic rocks, indicating that it joined the other minerals late in general but was on the liquidus throughout crystallization of the most silicic magmas.

We divide the batholith into six units that are distinct in texture, field relations, and in some cases compositions. These include a small exposure of the moderately felsic *roof unit* at one corner of the western margin the batholith; the *Spirit Mountain granite,* which is by far the most extensive unit; *Mirage granite,* which forms a discrete pluton; *diorite sheets* that are locally abundant; *fine-grained granite* that cuts most other units as thin to thick sheets; and the mafic to felsic *Newberry Mountains dike swarm,* the latest intrusions into the batholithic system. The petrology and field relations of each unit are discussed below.

Roof Unit

The roof unit is a small granitic section exposed over an area of ~3 km^2 at the northwest corner of the batholith, in contact with gneiss that forms the roof. It is a fine to medium-grained, pink granite with typically ~40-50% alkali feldspar (anhedral), 30% quartz (anhedral), up to 15-20% plagioclase (anhedral), <1% biotite (sub-euhedral), and ~1% opaques (a majority of which replace sphene and biotite). Plagioclase, alkali feldspar, and round quartz phenocrysts are present locally, none exceeding 5 mm in diameter. Myrmekitic intergrowths of quartz and plagioclase are very abundant in this unit.

Spirit Mountain granite

By far the largest unit of the SMB will be referred to as the Spirit Mountain (SM) granite. It dominates both the well-exposed western area and the less exposed, more altered northeast. In the western area, it constitutes a sequence that ranges from west to east, for the most part gradationally, from high-silica leucogranite into foliated quartz monzonite.

The western, or upper, margin of the SM granite (and thus of the batholith, except where the roof unit is exposed) is a ~25 km x 2 km zone of high-silica leucogranite. This zone comprises a collection of initially subhorizontal sheets of aplite, porphyry, and fine- to medium-grained, equigranular granite, with contacts that are sharp to barely perceptible. We interpret these relations to indicate repeated emplacement of the leucogranites - some sheets intruding a hot, melt-bearing mush, and some intruding solid rock. Vesicles, or miarolitic cavities, are widespread and commonest toward the west (top). Pegmatite pods and dikes dominated by coarse quartz and alkali feldspar are present locally. Typical leucogranites have ~40-50% alkali feldspar (subhedral), 30-40% quartz (anhedral in groundmass, but phenocrysts are subhedral), ~10 % plagioclase (sub-euhedral), and ~1% biotite (euhedral). Porphyritic variants contain ~0.5 cm phenocrysts of quartz and alkali feldspar.

The base of the leucogranite grades into coarser, less felsic granite over a distance of about 10-20 meters. Alkali feldspars become pink, biotite becomes more abundant, and quartz decreases in abundance. This coarse granite, which extends downward for ~3 km, averages ~20-35% plagioclase (euhedral laths), 30-40% alkali feldspar (sub-euhedral, ~1.5 cm), 15-30% quartz (interstitial and anhedral to ~1 cm subhedral), 5-8% biotite (euhedral), and ~1% sphene (euhedral). Quartz forms prominent, discrete, round grains to the west, but diminishes in size and abundance to the east (deeper levels). Rapakivi rims are evident on some alkali feldspar grains and become more abundant with depth. Locally, small (<2 cm), plagioclase + fine-grained biotite-rich clusters are present within the granite.

Fine-grained dioritic enclaves are present throughout the lower ~1/2 of the coarse granite. They range in maximum dimension from ~5-30 cm and are typically ellipsoidal, with irregular margins that are penetrated by crystals of the host granite, suggesting liquid/crystal mush (or mush/mush) contact. The enclaves are composed mainly of plagioclase and biotite, with minor hornblende and clinopyroxene. Some contain large alkali feldspars, suggesting crystal incorporation from the host granite. These enclaves are the only manifestation of mafic input during solidification of the SM granite unit. Schlieren are fairly common, with no recognizable trend. Many quartz-feldspar pegmatite pods are present in this granite. They tend to be bounded by schlieren, typically at their paleo-upper surfaces.

The coarse grained granite grades downward into magmatically foliated quartz monzonite that is poorer in quartz and richer in biotite. The quartz monzonite is coarse-grained, with 40-50% alkali feldspar (euhedral), 30-35% plagioclase (euhedral), 10-15% biotite (euhedral), and 5-15% quartz (interstitial, anhedral). Foliation, defined by aligned biotite, alkali feldspar, and plagioclase, gradually becomes stronger and is parallel to paleohorizontal. In this unit, dioritic enclaves are abundant, very large (up to 3m), pancake shaped, and oriented parallel to the rock's ~N-S striking, W-dipping fabric (Figure 3A). Based on euhedral to subhedral feldspar crystal shapes and weakly to unstrained interstitial quartz, this fabric is interpreted to be dominantly magmatic and probably related to compaction of a crystal mush (cf. Bachmann and Bergantz, 2004).

A distinct intrusive sequence marks a break in the gradation within part of the SM granite. This intrusion also grades from a high silica leucogranite cap (1-100 m thick) downward into coarser, less felsic granite. The contact between this unit and the overlying granite ranges from straight to very sinuous. A simple sharp interface divides the two units in places, while elsewhere, large vesicles (Figure 3B) and pegmatites are common at the contact. Locally, small (<m) blocks of the overlying granite appear just below the contact. We have been unable to locate the basal contact of this sequence, probably because of its similarity to the host granite. A network of leucogranite dikes

and sills (Figure 3C) emanates from the top of this intrusive sequence into the overlying SM granite. Large pods of leucogranite up to 500 m long by ~150 m thick, elongated in the paleohorizontal direction and bounded by sharp contacts on all sides, are present in the SM granite about 1 km above the distinct intrusive sequence. We interpret the leucogranite in these bodies to have originated from this intrusion, migrated upwards via dikes, stalled, and ballooned to form the present pods.

Mirage granite

The Mirage granite is separated from the SM granite by a thin (~5 to 50 m) septum of Proterozoic granite along part of the contact. Where a contact with SM granite is exposed, the Mirage granite cuts the SM granite foliation. Likewise, felsic dikes that appear to emanate from the Mirage granite intrude the SM granite. The granite is characterized by abundant quartz that is usually visible in hand sample to the unaided eye (<5 mm), and ranges in texture from very fine to medium-grained. The westernmost (upper) rocks near the contact with the SM granite are medium grained and have abundant quartz and a low biotite content (1-2%). Similar felsic granite is also present in sheets and pods (1-5 m thick) elsewhere in the Mirage granite. The interior of the Mirage pluton is medium grained, has less quartz, more biotite, and is characterized by ~2 cm alkali feldspar phenocrysts. The Mirage granite has a strong fabric in places, with polycrystalline stretched quartz indicating subsolidus deformation. Fine grained basaltic to medium grained dioritic pods and dikes cut and may locally mingle with the eastern (lower) part of the granite. These mafic intrusions may be associated with the dioritic rocks described below.

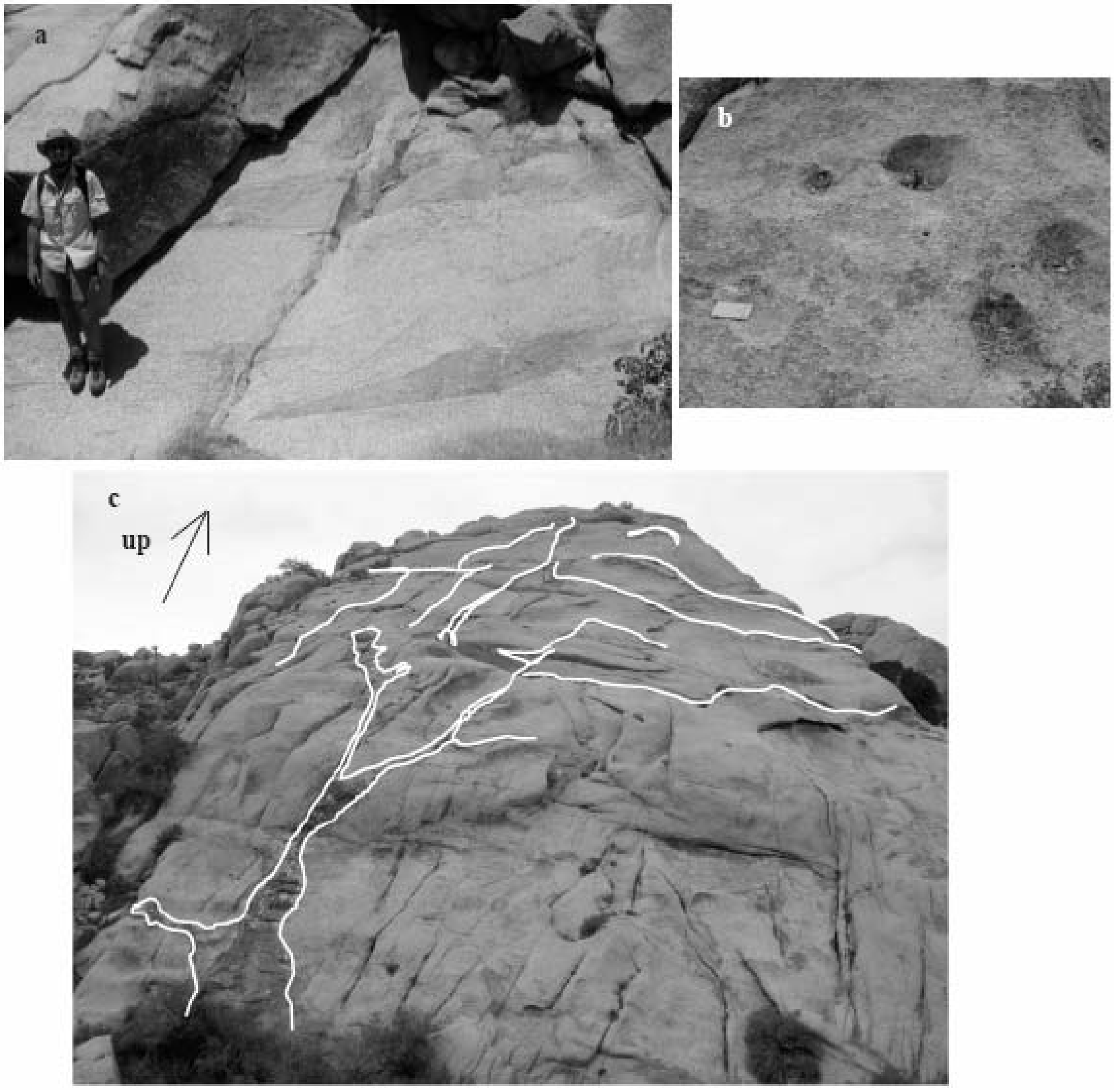

Figure 3: (a) Large, pancake-shaped mafic enclaves within the SM quartz monzonite. Enclaves are aligned parallel to the host's foliation. 5'9" Ben George for scale. (b) Large quartzofeldspathic cavities within the SM leucogranite. (c) A network of leucogranite dikes and sills within the SM granite. Paleo-up direction indicated.

Diorite sheets

Relatively mafic rocks, typically dioritic, are exposed as initially subhorizontal sheets to pod-like intrusions up to ~100 m thick that cut the deeper and more southerly parts of the SM granite. Locally, these sills pinch out and then reappear along strike. In places, the diorite is also present as pillows in the fine-grained granite unit (see below). Though visually striking, the diorite is, volumetrically, a very minor unit of the SMB. Blocks of the SM granite are present but sparse within the diorite bodies. While some granite blocks are angular and have sharp margins, others have irregular, poorly defined margins and the host mafic rock is contaminated by feldspar crystals, suggesting partial disaggregation of the granite (Figure 4A). At one well-exposed outcrop, many xenoliths can be seen in what appears to be a spectrum of disaggregation, from angular blocks to loose collections of feldspars within contaminated diorite (Figure 4B). At the same outcrop, a xenolith with a tail of contaminated rock might document the frozen process of floating in denser mafic magma, with the tail representing a wake of contamination and feldspar dissemination (Figure 4C).

The diorite is fine- to medium-grained, and typically contains close to 50% hornblende, over 50% plagioclase, <5% quartz, and up to 5% biotite. Sphene, apatite, opaques, and minor zircon are present as well.

Fine-grained granite

Like the diorite, the fine-grained granite (FGG) is observed primarily as subhorizontal sills to pod-like intrusions within the middle to deeper parts of the southern SM granite (cf. Hopson et al., 1994). Sharp cross-cutting relationships clearly show that

FGG intruded the SM granite. Blocks of the SM granite (in some cases perhaps disaggregated or *in situ* screens), ranging in size from cm's to >100 m, are common within the FGG. Individual FGG sills, where discernible, are cm's to 50 m thick, though in many places it is difficult to identify separate sheets. In some areas, internal contacts separate FGG phases that are distinguishable by the presence or absence of 1-2 cm alkali feldspar megacrysts. It is unclear whether these megacrysts were derived from the SM granite wall rock, or if they grew from the FGG magma.

In places, blobby pillows of diorite within the FGG (Figure 4D) indicate that intrusion of the two magmas coincided, but angular enclaves of diorite in FGG and sharp contacts of FGG dikes into diorite indicate that at least some of the FGG intruded after diorite became rigid. This, along with the internal contacts, suggests that there were multiple pulses of FGG emplaced into the SMB. Small dikes of the FGG cross cut portions of the Mirage granite, although a clear contact between the two units has not been established.

FGG is uniformly fine grained, equigranular, and uniform in appearance, except for the alkali feldspar megacrysts that distinguish it locally. It typically has 30-35% plagioclase (small, euhedral laths), 25-30% quartz (anhedral), 30-35% alkali feldspar (blebby, anhedral), and 5-10% biotite (euhedral). Myrmekitic intergrowths of quartz and alkali feldspar are common. Megacrysts of alkali feldspar where present have slightly irregular and inclusion-rich boundaries, perhaps indicating minor resorption followed by regrowth. At many locations, biotite is aligned and the quartz is strongly strained with conspicuous subgrain development, suggesting minor to moderate subsolidus deformation of the FGG unit.

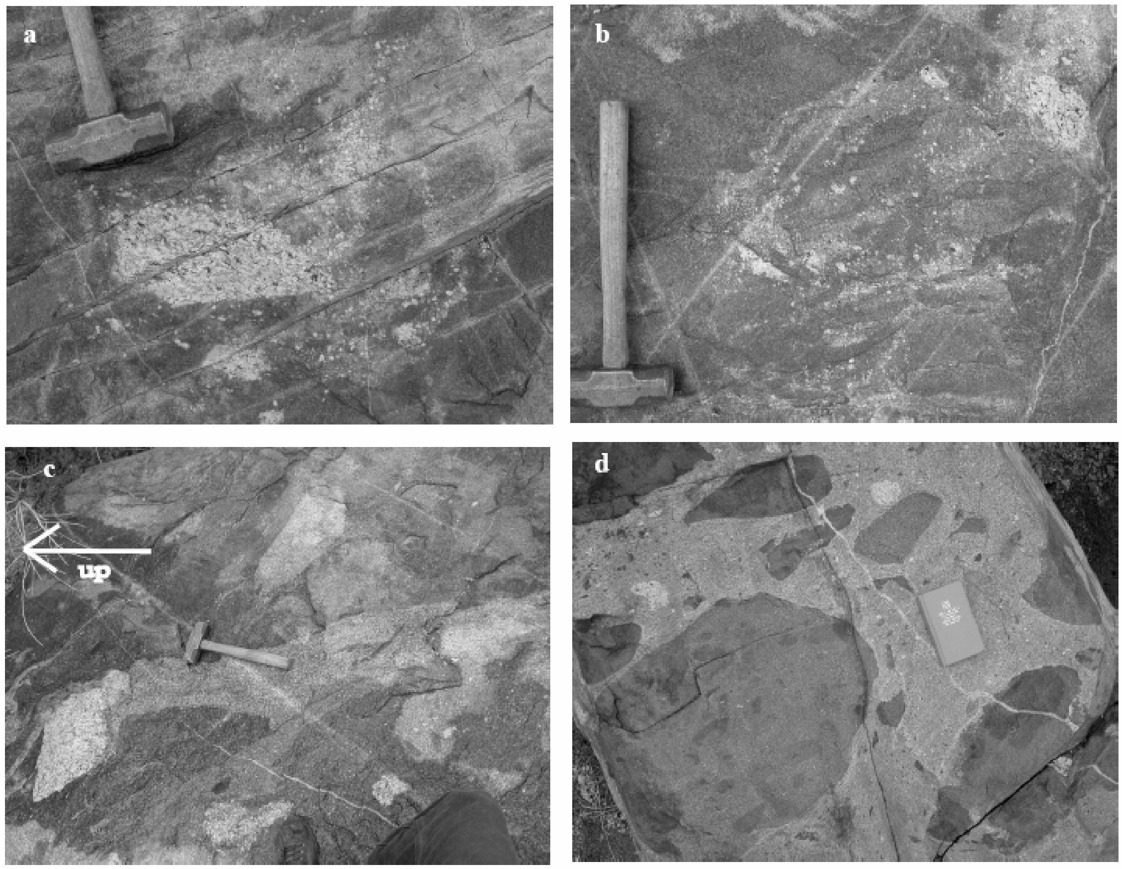

Figure 4: (a) A xenolith of SM granite within the diorite. Poorly defined margins of the xenolith and large feldspar crystals in the diorite suggest this xenolith was partially disaggregated. (b) A loose collection of feldspar crystals within a contaminated diorite perhaps documenting the final stages of xenolith disaggregation. (c) A SM granite xenolith with a tail of feldspar-bearing, contaminated diorite, possibly documenting the frozen process of a xenolith sinking (or floating) in the diorite. (d) Contaminated dioritic pillows within a contaminated fine-grained granite (FGG). Note also the small, white xenoliths of the SM granite.

Dike Swarm

The Newberry Dike swarm strikes ~N-S and cuts all other units in the SMB. Paleomagnetic data show that these dikes intruded roughly vertical and were rotated to ~40-65° E dips (Faulds et al., 1992; George et al., 2005). The dikes are aphanitic to fine-grained phaneritic and range in composition from granitic to basaltic. The felsic dikes are ~3-20 m thick, whereas most of the mafic dikes are ~1-5 m thick (one unusual mafic dike is 15 m thick). The felsic dikes are porphyritic and contain up to 10% each of quartz, alkali feldspar, and plagioclase phenocrysts. Rounded quartz phenocrysts, though smaller than some of the euhedral feldspars (~3 mm vs. up to 1cm), are distinctive and prominent. Felsic dikes contain up to 5% biotite phenocrysts within a gray groundmass that comprises 60-80% of the rock. Typically, the dikes are more phenocryst-rich in their interior than at the margins. The mafic dikes are rich in plagioclase and hornblende (some with clinopyroxene cores) and contain variable amounts of biotite; most are fine-grained phaneritic, and phenocrysts are sparse to absent. In most places, the contacts between the dikes and the host are sharp and the dike margins are chilled. At one location, however, the contact between a felsic dike and the FGG locally interfingers, suggesting that the dike sufficiently remobilized the FGG to allow for magma interplay to occur. These dikes represent the last pulse of magma that was emplaced into the SMB.

CHAPTER V

GEOCHEMISTRY

The granitoid rocks of the SMB (excluding the mafic lithologies - dioritic sheets, late mafic dikes, enclaves) exhibit a broad, coherent range of chemical compositions (Appendix C). Silica contents range continuously from 63-79%, and major element Harker diagrams show predictable trends, with those elements compatible with the early mineral assemblage falling with increasing SiO_2 and those (few) that are not compatible rising (Figure 5). The SM granite encompasses the entire spectrum of granitoid compositions, with high-silica granite and quartz monzonite constituting the extremes. Other felsic units display far more limited chemical variation (FGG: 71-74 wt% SiO_2; Mirage granite: 73-74 wt% SiO_2; felsic dikes: one with 69 wt%, all 6 other analyses 72-73 wt% SiO_2).

Chondrite-normalized rare-earth element (REE) patterns for all granitoids are for the most part broadly uniform (Figure 6), with enrichment in light REE (40 – 600 x chondrite), negative Eu anomalies, and flat middle to heavy REE. In detail, there are striking differences for different lithologies. The lower-SiO_2 granitoids have the highest light REE and small Eu anomalies, whereas the high-silica granites have the lowest light REE, very large negative Eu anomalies, and depressed middle REE.

Granitoid samples with <~70-72 wt% SiO_2 show textural evidence for accumulation of feldspars, biotite, and accessory minerals (see Chapter 4), and they are enriched in elements that would be concentrated by accumulation (see Figures 5 and 6).

They have high Ca, Al, Ba, Sr, and Eu (corresponding to feldspar accumulation), Fe and Mg (biotite and oxides), and Ti, P, Zr, and light REE (accessory sphene, apatite, zircon, allanite, chevkinite). In contrast, the most silicic rocks are low in all of these elements and extremely depleted in Sr and Ba (to <10 and <20 ppm, respectively) and Eu. Their relative depletion in middle REE is attributable to extraction of sphene. Very low Zr/Hf (17-30) in these highly silicic rocks demonstrates fractionation of zircon (Miller et al., 2005; Lowery et al., in press). Samples with less than about 74 wt% SiO_2 have textures suggesting that quartz was a late-crystallizing phase, whereas those with >~74 wt% appear to have had early quartz. Two samples of quartz monzonite fall off the trends for K_2O and to a lesser extent other elements. One of these samples is K_2O enriched and also has high Ba, whereas the other has low K_2O and Ba, suggesting that they reflect local mechanical concentration or depletion of alkali feldspar.

The almost indistinguishable elemental chemistry of the FGG, Mirage granite, and late felsic Newberry dikes suggests that felsic magma input during the latter stages of batholith construction was highly uniform. Although none of the SM granite samples appears to reliably reflect input magma composition (instead, their textures and compositions indicate crystal accumulation and melt fractionation), the composition of the suite as a whole is consistent with derivation from magma very similar to the FGG-Mirage-felsic dike compositions.

The mafic rocks (diorites, late dikes, a single enclave analysis) range in silica content from 53-59 wt% and have compositional trends that appear to be unrelated to the

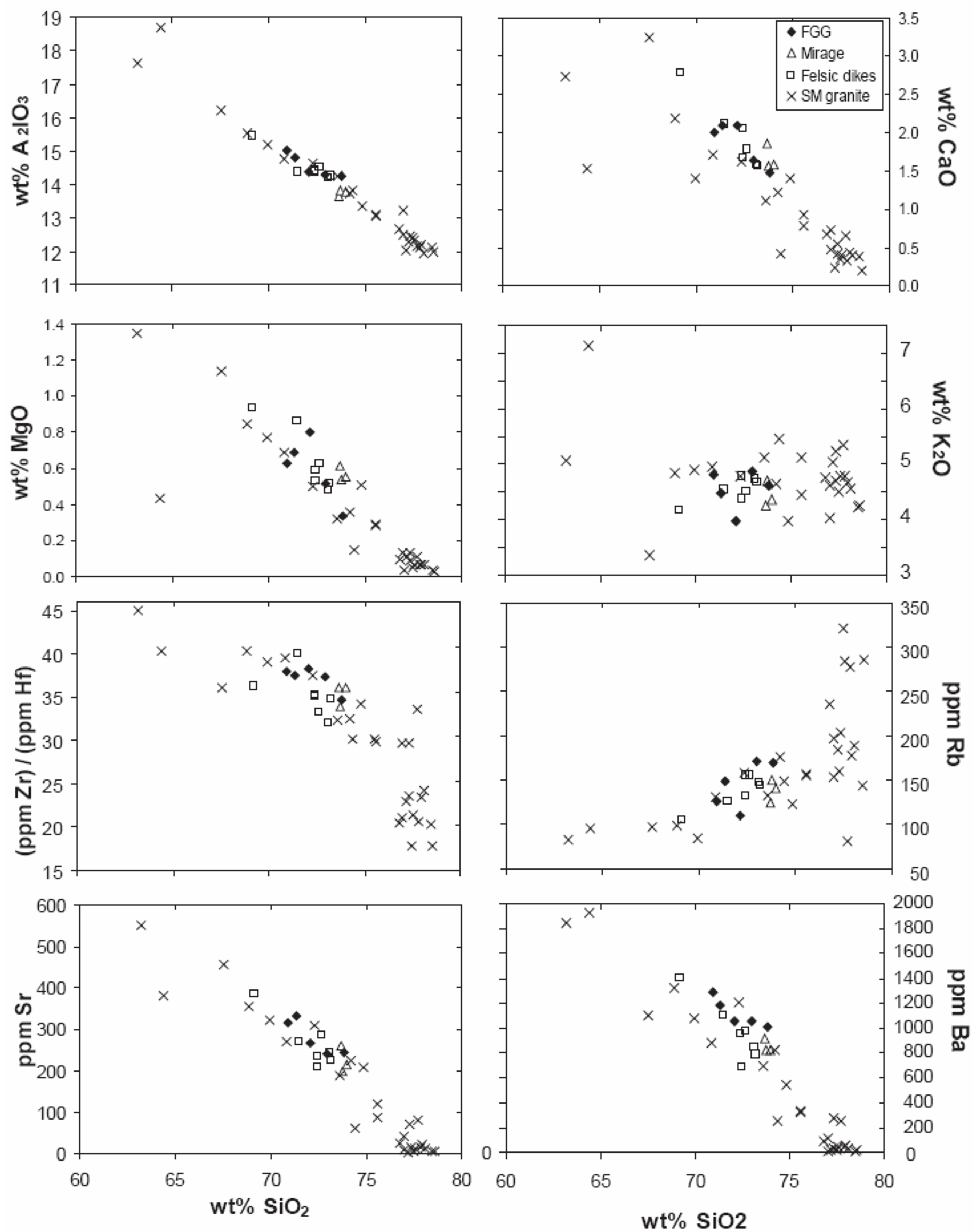

Figure 5: Harker diagrams for selected major element oxides and trace elements of SMB rocks with 60-80% SiO_2.

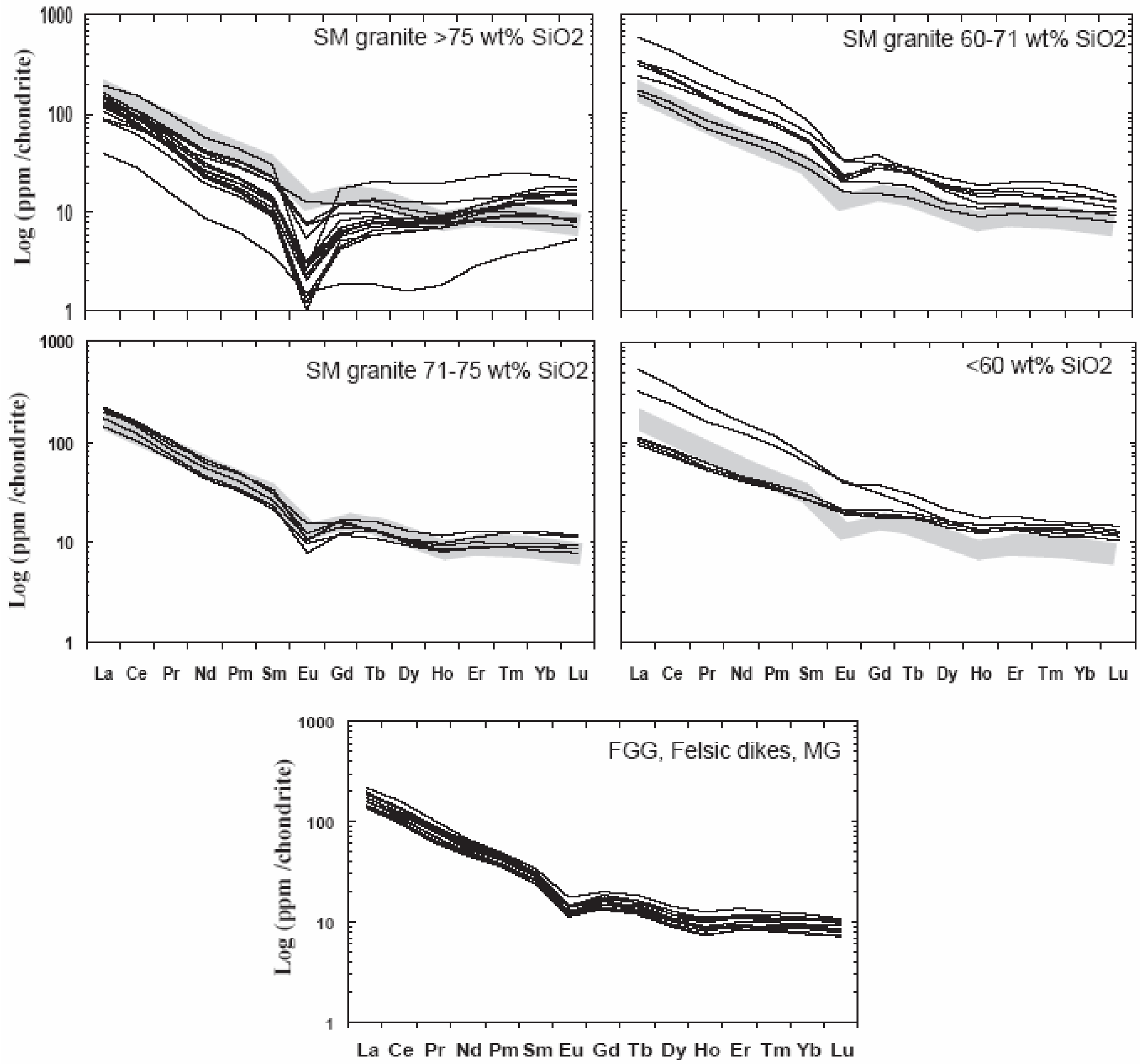

Figure 6: Chondrite normalized rare earth element patterns for the SMB samples, separated as indicated. The field for FGG, felsic dikes, and MG is shaded for comparison to the SM granite and mafic samples.

granitoids (Figure 7). They are relatively enriched in incompatible elements for mafic rocks, as is typical of the CREC (Metcalf, 2004).

Zirconium concentrations range from 50-600 ppm, except for the dioritic enclave, with 900 ppm. They correlate negatively with SiO_2 in the granitoids, as would be expected for accumulation of early zircon and falling zircon solubility in lower-T melts. Zircon saturation temperatures (T_{Zr}) for granitoids range from 700-880º C (Watson and Harrison, 1983). The lower values (<770º C) are for the high-silica granites and probably reflect melt segregation temperatures; the moderate-SiO_2 granitoids (including FGG, Newberry dikes, and Mirage granite, as well as some of the SM granites) have T_{Zr} of 770-810º C, which may approximate the T of input magmas. Highest T_{Zr}'s are for rocks that accumulated zircon and therefore are unrealistic (cf. Miller et al., 2003).

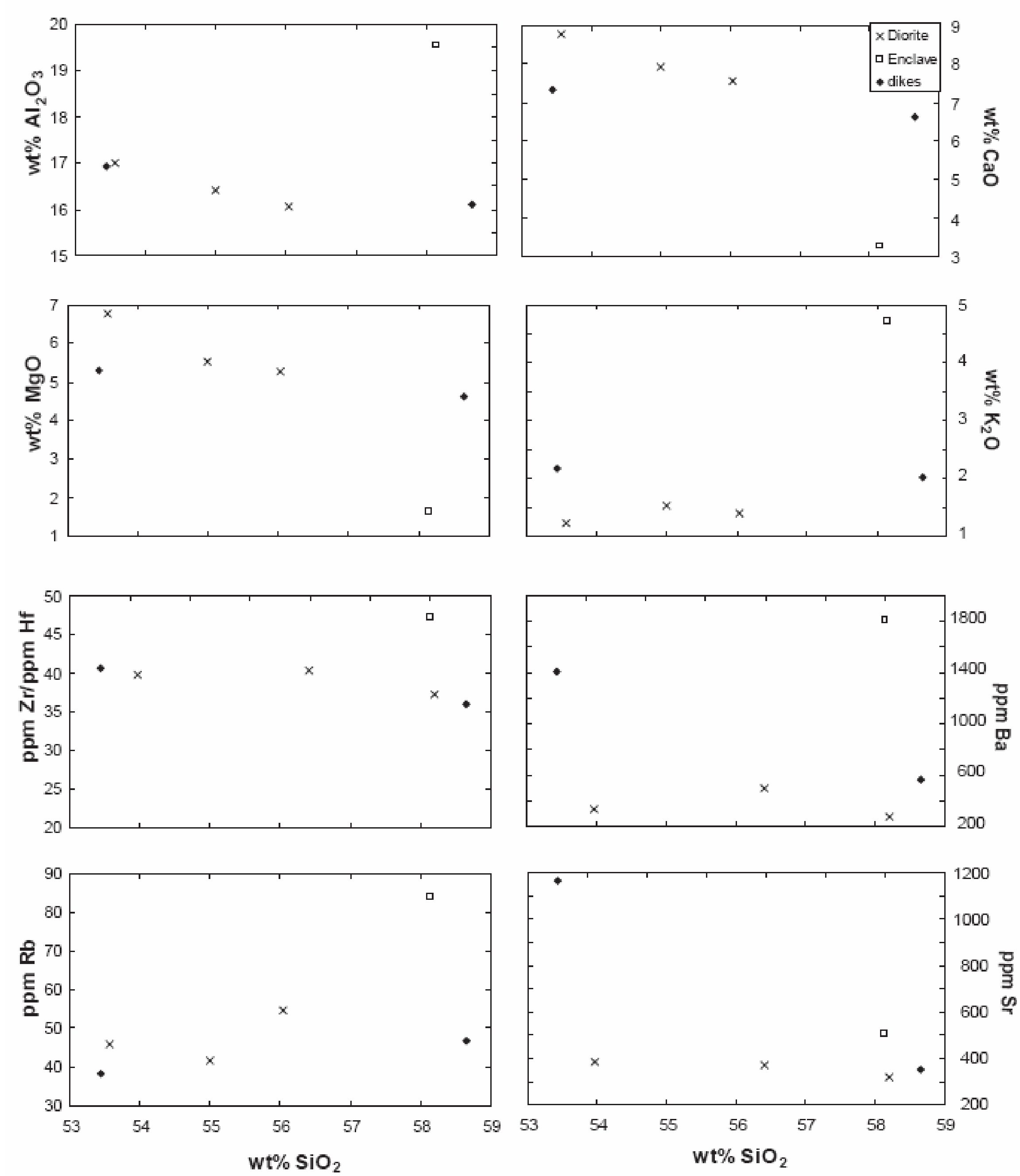

Figure 7: Harker diagrams for selected major element oxides and trace elements of SMB mafic rocks.

CHAPTER VI

GEOCHRONOLOGY

Conventionally, the expectation has been that dating magmatic zircons yields the age of crystallization of an intrusion (or at least the portion of the intrusion represented by the analyzed sample). Determination of this age may be hampered by Pb loss or by inheritance of older, unrelated grains, but it has been assumed that if these complexities can be eliminated, the "true" age of a sample (and the intrusion of which it is a part) can be ascertained. With the recent advent of much higher-precision "conventional" (thermal ionization mass spectrometry) analysis (e.g. Coleman et al., 2004), high-resolution ion probe dating (e.g. Cates et al., 2003; Miller et al., 2004; Miller and Wooden, 2004), and U-series disequilibria dating of young volcanic zircons (e.g. Charlier et al., 2005; Reid and Vazquez, 2002), it has become apparent that zircon ages in plutons and volcanic rocks may span a measurable range. Furthermore, individual samples may contain zircons that span much of this range. Our U-Pb data for the SMB further document the potential for identifying a crystallization age spectrum for a plutonic system and mixing of zircons of different ages within single samples. Wes Hildreth (presentation at Penrose Conference, 2001) coined the term "antecryst" for grains that are older than the solidification age of their host rock, but apparently represent earlier growth in the history of the system (Bacon and Lowenstern, 2005; see also “crystal memory” in Reid and Vazquez, 2002). These grains are presumably entrained by a younger magmatic pulse and then accumulate with newly formed/forming grains. This term and the concept it represents are critical for interpretation of SMB zircon data.

In interpreting our data, we rely on ^{207}Pb-corrected ^{206}Pb/^{238}U analyses. We assume that these very young zircons are concordant, because radiation damage and Pb loss are unlikely with such young grains, and CL images and U-Pb analyses of many cores suggest that inheritance (older than Miocene) appears to be present in only one sample. The ^{206}Pb/^{238}U ages are inspected directly, and we used routines in Isoplot 3.0 (Ludwig, 2003) that (1) seek single, statistically coherent populations representative of all or most of the data; (2) plot the data as probability density graphs, which reveal dominant and secondary age peaks; and (3) discriminate statistically meaningful populations from the age spectra (UNMIX, after Sambridge & Compston, 1994). Figure 8 shows typical CL images of SMB zircons. Figure 9 shows probability distribution plots of each SMB zircon sample, with UNMIX-identified populations indicated where applicable. Table 1 presents our interpretation of these data.

Excluding four inherited Mesozoic cores from a Newberry dike sample, essentially all individual analyses fall between 15 and 18 Ma, with obvious dominance between 15.5 and 17.5 Ma. We argue that this dominant range of ages is real. Specifically, we conclude the following (see Table 1):

(1) The roof unit sample SML59z yielded the oldest age, 17.4 ± 0.2 Ma, and a relatively simple age spectrum. This sample appears to represent a remnant of an early, perhaps initial, intrusion of the batholith preserved locally at the roof. Several younger ages in this sample may mark partial rejuvenation and zircon growth between 16-17 Ma.

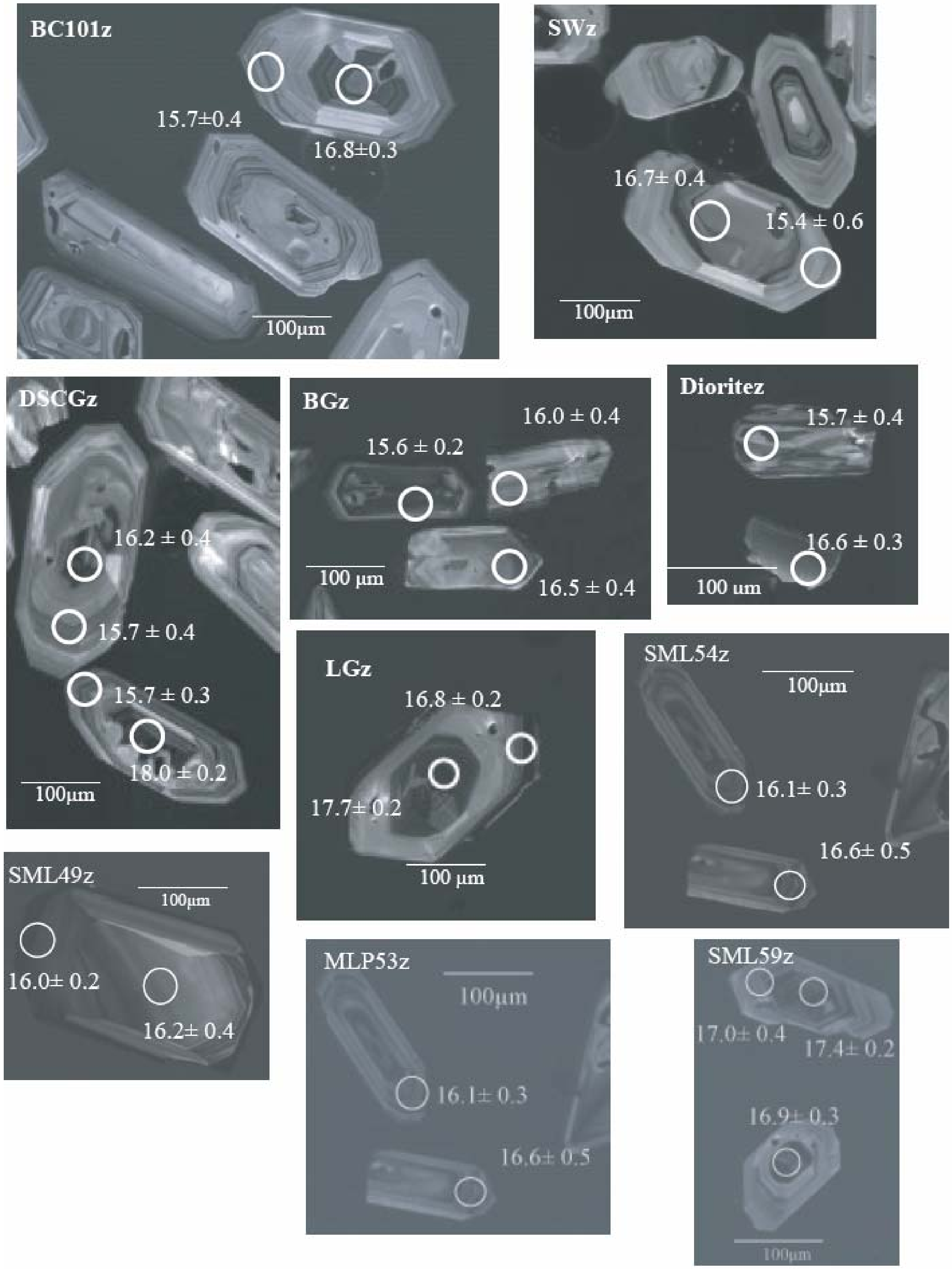

Figure 8: Cathodoluminescence images of SMB zircons from various samples. Ages are in Ma, and are 206Pb/238U. Errors are 2 sigma. Circles show approximate spot size and location.

(2) All samples that represent units that are demonstrably young (based on field relations) appear to be 15.3-15.9 Ma. (FGG, diorite, Mirage granite, Newberry dikes)
(3) All samples of SM granite have at least a major population between 16 and 17 Ma. In detail, it appears that there is a span of ages in this range that represents crystallization of a majority of the zircon in the batholith and, probably, solidification of most of its mass.
(4) All samples except roof unit SML59z appear to contain multiple zircon age populations. Most of the "extra" populations are probably composed of antecrysts. In some cases, though, the principal age of solidification may have been an earlier population, with a later population representing renewed, essentially *in situ* growth as a consequence of heating that accompanied magma recharge (see Table 1).
(5) One or more analyses from almost all samples yield ages of 17-18 Ma, suggesting wide redistribution of zircons from the earliest stages of batholithic growth (possibly represented by SML59z).

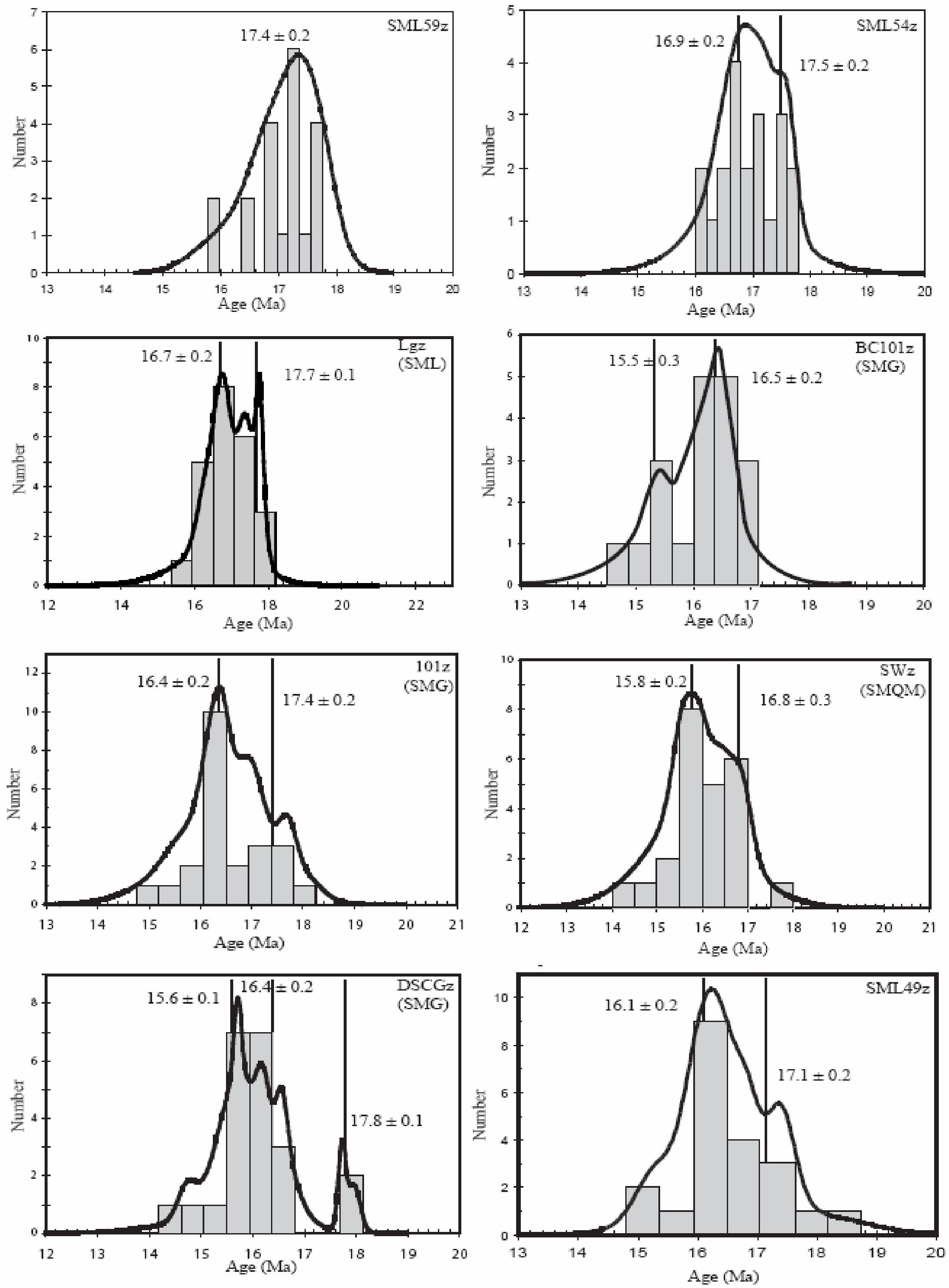

Figure 9: Probability density plots of SMB zircon samples. Vertical lines behind histograms indicate age populations, each of which is labeled with a date that was established by UNMIX (after Sambridge and Compston, 1994) in Isoplot. SML—leucogranite. SMG—granite. SMQM—quartz monzonite.

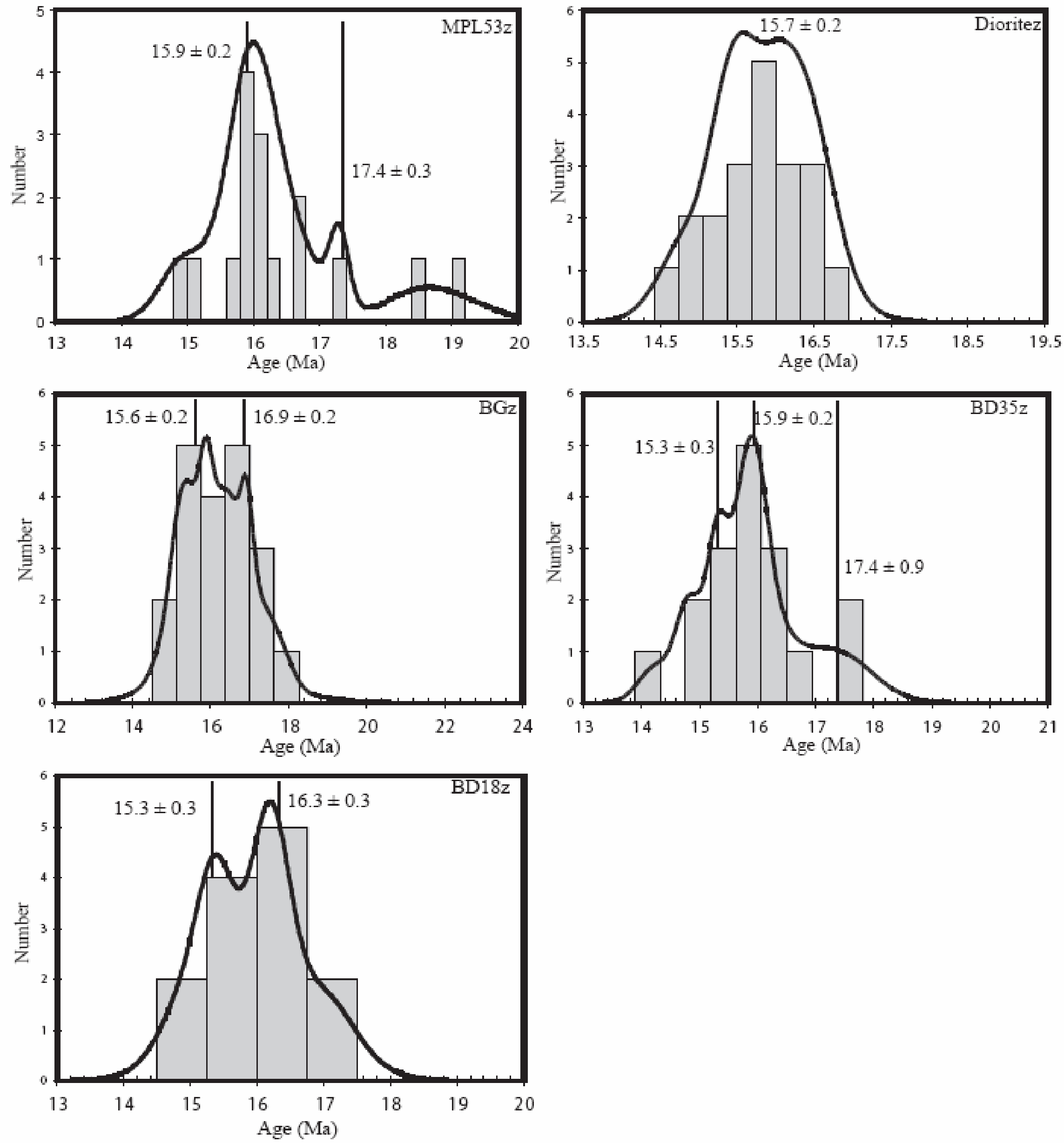

Figure 9: Continued. Probability density plots of SMB zircon samples. Vertical lines behind histograms indicate age populations, each of which is labeled with a date that was established by UNMIX (after Sambridge and Compston, 1994) in Isoplot. MPL—Mirage pluton. BGz—fine-grained granite. BD—felsic dikes.

Table 1: Synthesis of the Spirit Mountain batholith zircon samples.

Sample	Location Lat/Long	Rock type	No. of analyses	Inferred Age, ±2σ	Basis	Other populations	Comments
SML59z	114.7269, 35.2559	Roof unit	20	17.4 ± 0.2 Ma	Dominant peak of the data set with a ~Gaussian distribution.	none	
LGz	114.7461, 35.2594	Porphyritic SM leucogranite	23	16.8 ± 0.2 Ma	Dominant peak identified by UNMIX	17.7 ± 0.1 Ma	apparent antecrysts 17- 18 Ma abundant
SML49z	114.7869, 35.1364	Med grained leucogranite	21	16.1 ± 0.2 Ma	Dominant peak of the data set.	17.1 ± 0.2 Ma	Older population appears to be comprised of antecrysts.
SML54z	114.7428, 35.1817	SM granite - transitional leucogranite/ granite	22	16.8 ± 0.2 Ma	Dominant peak of the data set.	17.5 ± 0.2 Ma	
101z	114.6280, 35.2269	SM granite	23	16.4 ± 0.2 Ma	Dominant peak identified by UNMIX	17.4 ± 0.2 Ma	apparent antecrysts 17- 18 Ma abundant
BC101z	114.7139, 35.1996	SM granite	19	16.5 ± 0.2 Ma	Dominant peak identified by UNMIX	15.5 ± 0.3 Ma	Younger peak may reflect late heating by recharge, with accompanying zircon dissolution and new growth.
SWz	114.6655, 35.2400	SM quartz monzonite	24	16.8 ± 0.3 Ma or 15.8 ± 0.2 Ma	Two populations identified by UNMIX, Younger is dominant peak, older is prominent shoulder.		Older ages are generally in the cores/interior of zircons, younger ages in rims and interiors. May be part of the younger sequence within the SM granite and carry abundant antecrysts, OR it may be an older part of the SMg and show evidence for zircon dissolution and new growth as consequence of recharge.
DSCGz	114.6928, 35.2028	SM granite - within the younger intrusive sequence	22	15.7 ± 0.2 Ma	Dominant peak of the data set. Age consistent with field relations showing this sample as part of later sequence within SM granite	16.4 ± 0.2 Ma 17.8 ± 0.1 Ma	~15.7 Ma analyses are primarily on rims, though present in a few interiors. Apparent antecrysts mostly comprising cores/interiors.
MPL53z	114.6926, 35.1225	Mirage granite	17	15.9 ± 0.2 Ma	Dominant peak of the data set.	17.4 ± 0.3 Ma	Oldest Miocene grains in the SMB present in this sample: 18.5 Ma, and 19.1 Ma.

Table 1: Continued.

Sample	Location Lat/Long	Rock type	No. of analyses	Inferred Age, ±2σ	Basis	Other populations	Comments
Dioritez	114.6676, 35.1788	Fine-med grained diorite	20	15.8 ± 0.2 Ma	Mean of analyses – excludes 4 antecrysts(?) and a single anomalously young age (not recognized by UNMIX)	~16.3 Ma?	Several apparent antecrysts 16-17 Ma. Most grains lack euhedral, oscillatory zoning that characterize other samples (typical of zircons crystallized from mafic magmas)
BGz	114.6788, 35.1705	Fine grained biotite granite	20	15.6 ± 0.2 Ma	Largest peak, identified by UNMIX – many older grains interpreted as antecrysts	16.9 ± 0.2 Ma	There appear to be multiple ages of antecrysts, 16-18 Ma
BD18z	114.6878, 35.2025	Porphyritic felsic dike	18	15.3 ± 0.3 Ma	Most plausible of 2 subequal populations from UNMIX – field relations demonstrate youth, many zircons derived from SM granites relations.	16.3 ± 0.3 Ma 17.0 ± 1.1 Ma	Abundant "antecrysts;" 4 Mesozoic cores (170, 102, 99, 72 Ma)
BD35z	114.7075, 35.1798	Porphyritic felsic dike	18	15.3 ± 0.3 Ma	Relatively small population identified by UNMIX – but most plausible age, given field relations.	15.9 ± 0.2 Ma 17.4 ± 0.9 Ma (3 analyses 14.2-14.8 Ma interpreted to be implausible)	Abundant SM-age "antecrysts"

CHAPTER VII

DISCUSSION

Gradational granite: Simple appearance, complex history

The SMB is composed of multiple, discrete intrusions and was assembled over a protracted period. Field evidence for pulsatory construction is clear in some areas, as younger intrusions (Mirage granite, FGG, diorites, Newberry dikes) are clearly discernible. Geochronology supports the interpretation of this relatively late-stage growth of the batholith. In contrast, the SM granite, which comprises a majority of the batholith, appears to be a massive unit with a simple, monotonic history (Hopson et al., 1994). Based on its upward gradation from cumulate-textured quartz monzonite through coarse granite into highly evolved, fine-grained leucogranite, it could be viewed as a type example of a single-stage compacted cumulate with a segregated cap of high silica rhyolite equivalent (cf. Bachmann and Bergantz, 2004; Bachl et al., 2001). However, zircon geochronology suggests this unit developed over a span of a million years, longer than the plausible lifetime of even a magma batch of this volume. Furthermore, the distribution of ages is far from defining the pattern expected for a monotonic history (see Figure 2). Under close scrutiny, field relations also contradict this simple scenario and are instead consistent with a multi-stage intrusive history.

The six dated samples of SM granite all have at least two age populations of zircons. In most samples, the populations that comprise the minor peaks consist of older grains (or areas within grains), which we interpret to be antecrysts. The common presence of antecrysts indicates that an appreciable fraction of zircons (and presumably other phases from preceding pulses as well) was recycled into subsequent injections. Elemental zoning within the zircons, which documents major fluctuations in temperature and host melt composition, strongly supports this complex history for individual zircons and zircon populations (see Lowery et al., in press, cf. Ti-in-zircon thermometry; Watson and Harrison, 2005). This recycling suggests an explanation for the rarity of sharp contacts in a unit whose crystallization age spans a million years. Intrusion of fresh magma could effectively remobilize an area within a stagnant, crystal-rich mush pile. The resulting physical interaction could effectively obscure evidence of the injection and erase earlier contacts as well. Segregation of fractionated, interstitial melt may result from mush compaction, or it could be a consequence of destabilization of stagnant mush during recharge. The buoyant high-silica melt would then migrate upwards by porous flow or via tears (dikes) through the crystal-rich mush.

We envision a large pile of crystal-rich mush that buckled (compacted) under its own weight. This compaction reduced the pore space and subsequently caused a portion of the residual interstitial melt to evacuate these shrinking reservoirs (Bachmann & Bergantz, 2004). The resulting cumulate was enriched in the earlier crystallizing phases (feldspars, biotite, accessories), and depleted in quartz, a late crystallizing phase. This process would plausibly have the most impact on the bottom of the mush pile, where the pressure is the greatest. This could explain the large zone of quartz monzonite at the bottom of the SM granite, which is (1) enriched in feldspars, biotite, and accessories, (2) depleted in quartz, and (3) strongly foliated perpendicular to the up direction.

The other chemical extreme of the SM granite, the high silica leucogranite zone, also documents protracted assembly. Zircon samples from this unit (LGz, SML54z, SML49z) yield ages that bracket most of the life span of the SM granite (16.1-16.8 Ma). Field relations indicate that many pulses of high silica granite were emplaced at the roof as horizontal sheets. This suggests that segregation events occurred throughout the assembly of the SM granite. Ascent pathways for these fractionated melts (i.e. feeder dikes) are only rarely preserved within the SM granite, probably because they were disrupted by subsequent destabilization of the host mush or because they collapsed after drainage of melt.

The final product of a protracted history of repeated intrusion, mush destabilization, and melt segregation is the SM granite: a gradational, relatively homogeneous body with only subtle internal contacts. Little evidence for the initial form of intrusive pulses was preserved. The distinct, younger intrusive sequence within the SM granite is probably a manifestation of magma injection into a more mechanically sturdy medium, the previously emplaced portion of the SM granite being rigid enough to allow for the preservation of intrusion geometry.

Architecture of Construction

The composite, multi-stage constructional architecture of the SMB hinted at by the SM granite is made clearer by the younger units. The diorites and the FGG are exposed as hundreds of initially subhorizontal sheets, essentially exhibiting sill-on-sill geometry (Figure 10). This arrangement is similar to that described by Westerman and others (2004), who used the term “Christmas-tree laccolith" to describe a sheeted body on

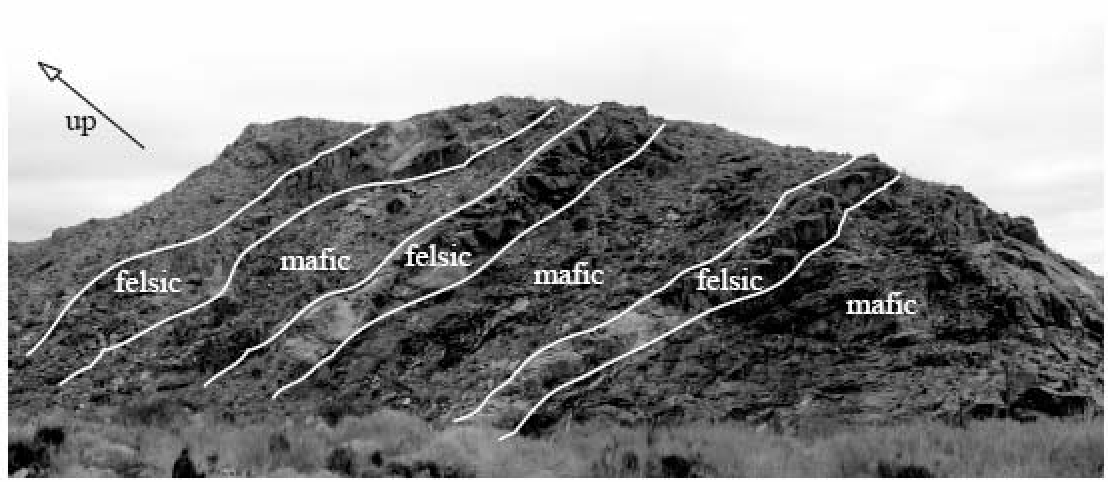

Figure 10: Successively stacked fine-grained granite (FGG) sills intruded into diorite. This sill-on-sill geometry is observed throughout the FGG and diorite units. For scale, the FGG sills are ~5m thick. Initial up direction is indicated.

Elba Island, Italy. Hunt (1953) described a complex assemblage of subhorizontal (laccolithic) sheets and subordinate dikes and protrusions in the Henry Mountains, Utah, as a "cactolith." Though partially in facetious reference to the increasing amount of geological jargon, Hunt was graphically describing a branching, cholla cactus-shaped intrusion. His description and his term evoke a pattern similar to what we observe in the SMB. This geometry applies not only to the FGG and diorite sheets, but also to networks of leucogranite dikes, sills, and laterally extensive pods within the SM granite both within the main mass and in the upper leucogranite zone; these networks presumably reflect accumulation of late, fractionated melts. We consider it likely that *initial* intrusions with similar sheet-like geometry merged through time to form the SM granite and the Mirage pluton - probably as a consequence of larger magma flux and therefore thermal mass, permitting more time to rework initial intrusion boundaries.

Assembly Sequence

Taking into account the field relations just discussed and the zircon geochronology, we interpret the SMB history to be as follows (Figure 11):

1) ~17.4 Ma: The magma associated with the roof unit (SML59z) was emplaced, followed by a pause in magmatism. Zircons associated with this initial phase of emplacement were later redistributed throughout most of the batholith.

2) ~17-16 Ma: Sporadic injection and crystallization of granitic magma formed the bulk of the SM granite. Magma was probably emplaced as horizontal sheets within a semi-rigid crystal mush. Injections partially remobilized the surrounding area, entraining zircon antecrysts, and creating (small?) local magma chambers. Within these local chambers, fractional crystallization occurred, producing high-silica melt which migrated upward towards the roof. Minor amounts of mafic magma were injected intermittently, becoming small pods and/or mafic enclaves.

   (Geochronology alone cannot accurately establish an order of steps 3-6, as events fall within error of each other. Field relations and zircon data are consistent with the following sequence and approximate timing.)

3) ~16.0-15.8 Ma: The Mirage granite intruded, probably in sheet by sheet fashion. Fractional crystallization of this magma produced a leucocratic roof zone, similar to but much smaller than that of the SM granite. Injections of basaltic-dioritic magma formed horizontal sheets and pods that cut the SM granite and were in part coeval with the Mirage granite.

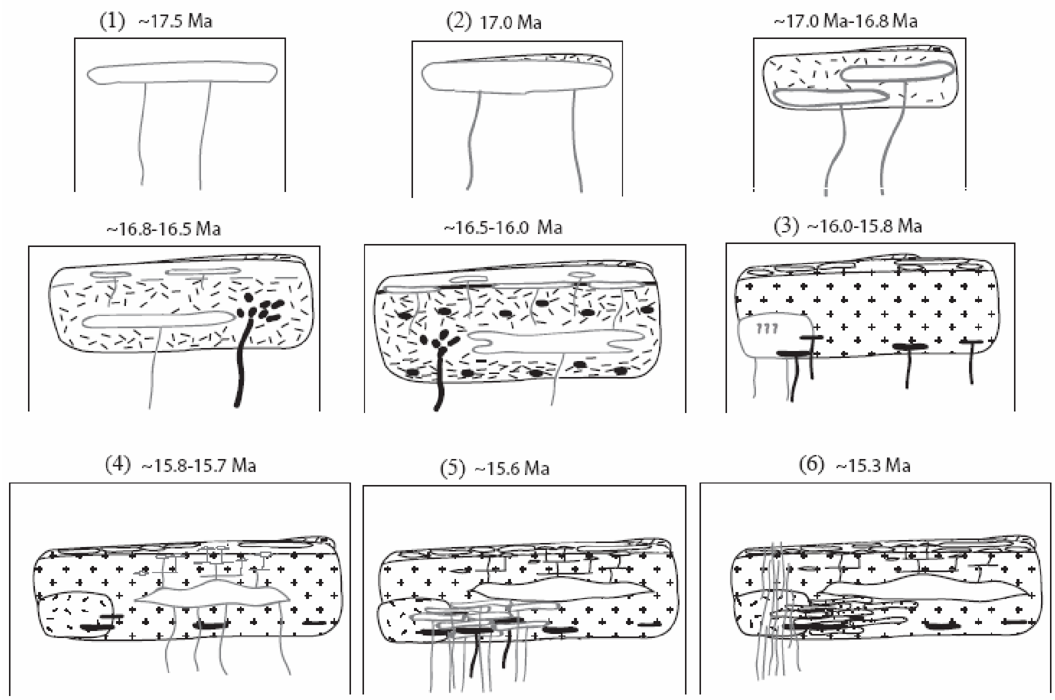

Figure 11: Assembly cartoon for the Spirit Mountain batholith. Numbers (1-6) correspond to explanation in text.

4) ~15.8-15.7 Ma: Magma continued to be injected into the SM granite, which had effectively solidified by this time, to produce the distinct, younger sequence. Fractional crystallization again produced high-silica melt which accumulated at the roof zone of this intrusion. Some of this fractionated melt debouched from the intra-batholith cupola, upward into the overlying granite. A preserved network of leucogranite dikes, sills, and pods document the ascent pathways and ponding zones of this material. This magma addition probably provided enough heat to the surrounding granite (mush?) to dissolve zircons (+ other minerals?) and grow new rims *in situ*.

5) ~15.6 Ma: FGG was emplaced as a series of successively stacked, horizontal sheets. Cooling of this injection was probably relatively rapid, as suggested

by the fine grained texture. Minor mafic-dioritic magma emplacement continued through this time, as well.

6) ~15.3 Ma: Termination of SMB magmatism was marked by injection of a series of vertically intruded, felsic to mafic dikes. Emplacement of the Newberry dike swarm followed final solidification of the remainder of the batholith and may have been facilitated by the onset of rapid E-W extension (George et al., 2005), which is suggested to have occurred ~15.5-16.0 Ma (Faulds et al., 2001).

CHAPTER VIII

CONCLUSION

Construction of a "Patchwork Batholith"

Piecemeal construction of the SMB is documented by zircon geochronology, field relations, and elemental geochemistry. These data demonstrate multiple injections, repeated melt segregation events, and remobilization and modification of early phases over a protracted period. The general pattern of the largest unit, the SM granite, is deceptively simple: a large roof zone of fractionated, high-silica leucogranite that grades though coarse-grained granite into a foliated quartz monzonite. Closer examination of this unit, though, reveals its more complex history. Zircon growth in the SM granite spans a million-year interval, zircon age populations are mixed within samples, and field relations reveal that both the fractionated leucogranite zone and the underlying portion record multiple injections. Younger, fine-grained granite and diorite are preserved as complex sets of sheets, resulting in "cactolithic" or "Christmas tree" geometries. We envision accumulation of horizontal sheets in this manner as the dominant process in the assembly of the SMB. Presumably depending on the consistency and temperature of the host, these sheets either froze relatively quickly to preserve a sharp geometry, or locally remobilized a crystal mush. Where remobilization occurred, original geometry was obscured, resulting in a relatively homogeneous mass. Thus, the shape of the batholith, with an aspect ratio of ~3, does not reflect its building blocks, which had far higher aspect ratios (cf. McCaffrey & Petford 1997, Glazner et al., 2004). At any given time, the batholith was a patchwork of melt-rich, melt-poor, and probably entirely solid zones. The location, size, shape, and melt fraction of the mush zones must have varied dramatically over the two million year history of the batholitic system.

Zircon samples from the SMB have age spectra that span the assembly time of the batholith, with dominant peaks in individual samples representing the time at which the host rock was largely consolidated. The older populations are most likely due to the recycling of zircon antecrysts into new injections of magma. In this way, each new injection might acquire memory of previous crystallization events. The patchwork nature thus ranges in scale from map view to hand sample and single crystal, with evidence for multiple injections ranging from contacts to U-Pb ratios in zones within individual zircons.

APPENDIX A

GEOLOGIC MAP OF THE SPIRIT MOUNTAIN BATHOLITH

(see file SMB_geologic_map.pdf)

APPPENDIX B

PETROGRAPHIC DESCRIPTIONS

Sample	Long.	Lat.	Rock Name	qtz	K-spar	plag	bt	hbl	sphene	opaques	acc.	alt'n	Description
BW02	114.7250	35.2047	granite	30	35	30	5		1	<1	al, ap, zir	chl, ser	Coarse grained, peppered with small plag grains. Very altered. Muscovite comprising the sericitic alteration is very coarse in places.
BW04	114.7120	35.2002	granite	20	30	35	15		<1	<1	ap, zir	chl, ser	Fine gr. Large Kspar phenos, with A gradational border. Phenos and surrounding interstitial Kspar are in optical cont. Small euhedral plag laths with 3:1 aspect ratio.
BW05	114.7050	35.1997	granite	30	35	30	5		<1	<1	ap, zir	ser	Medium grained. Fine grained component enclosed by coarser component. Most larger grains are feldspar. Rapakivi rim on one large Kspar pheno in optical cont. with plag in perthitic lamellae.
BW07	114.6987	35.1878	granite porphyry	65		30	5				zir,		Porphyritic. 60% matrix. Mineral %'s are for phenocrysts only. Quartz is large and round, plag is smaller and sub-euhedral.
BW12	114.6676	35.1788	diorite	5		50	5	40	<1	<1	ap, zir	chl	Medium grained. Sub-euhedral hornblende. An-subhedral plag. All biotite has been chloritized.
BW21	114.6494	35.2293	granite	30	29	35	5		<1	1	al, ap	chl, ser	Coarse gr. Thoroughly altered (all biotite has been chloritized). Brittle deformation is evident by heavily brecciated avenues.
BW24	114.6919	35.2651	leucogranite	35	40	25	<1			<1	zir	ser	Medium grained. Biotite enclosed by plag, which is enclosed by kspar. Quartz is anhedral and clearly late stage, although plentiful. Feldspars comprise larger grains.

Sample	Long.	Lat.	Rock Name	qtz	K-spar	plag	bt	hbl	sphene	opaques	acc.	alt'n	Description
BW26	114.6040	35.2396	altered granite	30	30	25	5			<1	ap, ep, zir	chl, ser, ep	Very altered, fractured granite, mostly med gr. All bt is chloritized. Ep replaces bt and feldspars in places. Kspar forms largest XLs/porphyroclasts (?).Biotite is aligned, and feldspars, to some extent, are too.
BW27	114.6972	35.2714	leucogranite	35	39	25	1			<1	zir	ser	Fine grained. Marginal phase of the SMB. Large Kspar phenos break up the otherwise homo-geneously fine gr texture. Myrmekite texture present.
BW29	114.6731	35.1849	granite	23	30	35	10		1	1	ap, zir	chl, ser	Fine gr with larger, sub-euhedral plag grains. Finer grained, elongated bt/sphene/opq/ap-rich enclaves present, characteristic of this phase. Quartz heavily subgrained.
BW30	114.6769	35.1864	granite	25	35	31	8		<1	1	ap, zir	chl, ser	Fine gr. granite with no large phenos. Some Kspars are a bit larger, though. Kspars zoned in places. Weak alt'n. Qtz anhedral, interstital. Opaques are blebby w/ a biotite affinity. Mild alingment of bt. Qtz is weakly deformed.
BW32	114.6542	35.1663	quartz monzonite	9	70	15	3		<1	<1	al, ap, zir	chl, ser	Coarse gr. Very rich in Kspar. Poor in quartz. Texture suggests Kspar accumulation. Biotite is foliated, aligned with the Kspar.
BW33	114.6571	35.1665	granite	17	45	28	9		1	<1	ap, al, zir	chl, ser	Fine grained with large feldspar phenos. Biotite aligned strongly. Quartz clearly deformed. A few phenos look rotated.

Sample	Long.	Lat.	Rock Name	qtz	K-spar	plag	bt	hbl	sphene	opaques	acc.	alt'n	Description
BW34	114.6677	35.1684	diorite	4		40	5	50	1	<1	ap, zir		Equigranular med gr. An- subhedral hornblende is present in clots. An-subhedral plag. Small pockets of quartzofeldspathic material are present.
BW36	114.7208	35.1992	granite	25	45	25	3		<1	<1	al, ap,zir	chl, ser	Coarse grained. Kspars big, blobby, and very perthitic. Plag is mostly smaller laths, subhedral.
BW37	114.7211	35.1992	granite	30	45	22	3		<1	<1	al, ap,zir	chl, ser	Coarse gr. Kspars big, perthitic, eu-hedral in places, mostly an-subhedral. Plag is smaller laths, euhedral. A conglomerate plag grain is present here. Some euhedral quartz is in this sample. Interesting qtz/kspar boundaries, with Kspar appendages forking into the qtz grains.
BW38	114.7050	35.1997	granite	30	33	30	5		1	1	al, zir	chl, ser	Med-coarse grained. Zoned subhedral plag. Large, perthitic Kspar laths some w/ rapakivi texture. Euhedral biotite. Anhedral quartz w/ prevalent intergrowths of other phases. Euhedral accessories.
BW39	114.7066	35.1997	granite	30	31	32	7		<1	<1	al,ap, ep,zir	ser	Med grained. Kspar comprises largest grains, but not all grains are large. Quite a bit of allanite, while not much sphene at all.
BW41	114.7107	35.2004	granite	30	26	33	8		1	1	al,ap, ep,zir		Texture is most interesting and heterogeneous. Profuse fine gr. plag and biotite XLs enclosed by large quartz and Kspar. Several large plag and one Kspar pheno. Med gr. granitic xenolith present, as well. Big felsdpars have "blobby cellular" texture. Plausible this sample experienced a 2 stage cooling history.

Sample	Long.	Lat.	Rock Name	qtz	K-spar	plag	bt	hbl	sphene	opaques	acc.	alt'n	Description
BW42	114.7116	35.2002	granite	30	25	38	6		<1	1	ap,zir	chl, ser	Fine grained with large euhedral plag phenocrysts. Small, euhedral plag laths. Anhedral quartz, Kspar. Weakly aligned euhedral bt. Myrmekite texture present.
BW43	114.7171	35.1995	granite	30	30	32	6		1	1	al,ap, ep,zir	chl, ser	Med-coarse grained, with euhedral biotite and plag. Large plag grains look to be conglomerates of many smaller "plaglets." Kspar grains are generally large and perthitic. Anhedral uartz. Fair amount of what appears to be magmatic epidote in this sample.
BW44	114.6873	35.2116	granite	20	50	25	4		<1	1	al, ap, zir	chl, ser	Coarse grained, with large Kspar crystals (plausibly accumulated). Quartz is clearly later, forming boxy crystals which grew up against euhedral feldspars.
BW45	114.6837	35.2095	granite	30	36	25	8			1	al, ap, zir	chl, ser	Fine gr., equigranular, except for two larger Kspar phenos. One large Kspar pheno appears to be microcline. Biotite mod. alligned. Crystals are generally an-subhedral. myrmekite present. Much allanite in this sample.
BW47	114.7102	35.1929	leucogranite	39	40	20	<1			1	musc	.	Fine-med grained. Rock dominated by graphic quartz-Kspar intergrowths. Quartz comprises skeletal mineral, Kspar is the intergrowth "matrix." Muscovite probably due to high F concentration (along with other volatiles) in magma. Biotite acicular.

Sample	Long.	Lat.	Rock Name	qtz	K-spar	plag	bt	hbl	sphene	opaques	acc.	alt'n	Description
BW49	114.6928	35.2028	granite	25	30	35	6	2	1	1	al, ap, zir,	chl, ser	Heterogeneous texture: fine to coarse gr. Apatite frequently enclosed by biotite. Large, subhedral Kspars exist, plag smaller, subhedral.
BW50	114.7013	35.2085	granite	25	35	33	6		1	<1	al, ap, ep, zir	ser	Med to coarse grained. Most minerals have small to larger grains in this sample, giving it an interesting, almost two-sized texture.
BW51b	114.6694	35.2420	leucogranite	40	55	25	2		<1	<1	al, zir	chl, ser	Coarse grained leucogranite. Quartz is deformed and concentrated in large domains. Kspar is perthitic and comprises larger grains. Smaller plag laths are subhedral.
BW62	114.6736	35.1684	granite	21	45	25	8		<1	1	al, ap, zir	chl, ser	Med grained. Deformed quartz and aligned biotite indicate strain in this sample. Large Kspar phenocrysts are present, but not strained. Plag is mostly euhedral and lath shaped.
BWen	114.6670	35.2412	dioritic enclave				25	5		2			Fine grained enclave. Large plag phenos (with many inclusions) are present, possibly incorporated from host granite. Apatite very abundant. Sample contains 5% clinopyroxene.

Sample	Long.	Lat.	Rock Name	qtz	K-spar	plag	bt	hbl	sphene	opaques	acc.	alt'n	Description
Lgz	114.7461	35.2594	leucogranite	40	49	10	1			<1	ap, zir		Large subhedral quartz and Kspar phenocrysts. The smaller grains almost comprise an equigranular matrix.
Bgz	114.6788	35.1705	granite	30	30	34	5		<1	1	al, ap, zir	chl, ser	Fine grained granite. Biotite alignment and quartz deformation indicate that this rock was subjected to post- (and plausibly) syn- crystallization stress.
101z	114.6280	35.2269	granite	25	40	25	7		1	2	al, zir	chl, ser	Coarse grained. Chlorite and sericite alteration is extensive (due to proximity to DP Mt fault). Kspars large, plag smaller. Quartz very deformed, interstitial.
MI-2	114.6927	35.1225	granite	25	40	26	9		<1	<1	al, ap, zir	chl, ser	Med grained with the exception of several larger Kspars which appear to be phenos, but in some cases have irregular boundaries. Biotite aligned moderately. Quartz is comprised of puzzle piece shaped subgrains.
SWz	114.6655	35.2400	quartz monzonite	10	65	10	5	7	2	1	al, ap, ep, zir	ser	Coarse grained. Kspar forms largest and most abundant grains. Mafic minerals appear together in clots between large grains. Boundaries of big Kspars are lined with microcrystalline quartz. This rock is very plausibly a compacted cumulate, which has had melt segregated from it.

APPENDIX C

MAJOR AND TRACE ELEMENT GEOCHEMICAL DATA

Sample	BW11	BW34	BW40	BW43	BW48	BW61	BW62	BW63	BW49
Longitude	114.6642	114.6680	114.7083	114.7171	114.7274	114.6707	114.6736	114.6928	114.6928
Latitude	35.1783	35.1684	35.1999	35.1995	35.2473	35.1687	35.1684	35.2028	35.2028
Rock type	FGG	diorite	SMG	SMG	SMG	diorite	FGG	FGG	SMG
SiO2	72.12	54.99	74.24	74.85	75.58	56.04	71.36	72.98	68.88
Al2O3	14.38	16.40	13.75	13.36	13.07	16.06	14.83	14.28	15.53
Fe2O3	2.39	8.48	1.59	1.72	1.35	7.86	2.40	1.90	2.94
MnO	0.04	0.13	0.05	0.05	0.05	0.13	0.05	0.04	0.06
MgO	0.80	5.54	0.36	0.51	0.29	5.29	0.69	0.51	0.85
CaO	2.10	7.92	1.22	1.40	0.93	7.57	2.09	1.64	2.18
Na2O	3.77	3.57	3.82	3.82	3.97	4.35	3.65	3.48	4.00
K2O	3.97	1.53	4.66	3.97	4.46	1.39	4.47	4.87	4.84
TiO2	0.34	1.22	0.23	0.25	0.23	1.13	0.35	0.23	0.53
P2O5	0.10	0.22	0.08	0.07	0.06	0.18	0.11	0.08	0.18
Rb	110	42	175	123	156	55	148	171	98
Sr	268	368	224	210	121	319	332	240	356
Ba	1063	494	820	541	341	279	1183	1053	1323
Cs	1.1	0.6	1.3	1.1	0.9	0.4	1.3	1.3	0.7
Ta	1.18	0.64	1.73	1.33	2.22	0.65	1.09	1.16	1.73
Nb	13.0	8.8	19.2	16.9	29.2	8.8	13.7	14.2	22.0
Tl	0.58	0.20	0.95	0.59	0.70	0.32	0.74	0.98	0.51
Pb	20	<3	21	18	25	7	4	22	20
Hf	4.4	4.8	4.9	4.4	5.1	4.3	4.7	4.9	7.7
Zr	167	193	160	152	153	160	172	180	312
Y	20	31	19	19	23	27	20	21	43
Sc	6.5	31.7	3.9	4.1	3.5	27.9	5.1	4.2	5.6
Cr	12.1	139	<0.5	4.0	5.2	149	6.7	7.6	6.7
Ni	7	62	3	3	3	3	65	6	7
V	29	157	16	14	13	145	29	17	37
Cu	7	45	4	1	4	35	36	7	6
Th	12.8	5.63	19.6	14.1	27.2	4.90	11.7	16.7	9.26
U	1.66	0.85	3.07	2.54	2.89	0.82	1.57	1.68	1.26
Ga	18	18	19	17	20	19	20	19	20
La	45.3	33.9	68.6	43.9	54.1	28.7	50.2	58.6	73.3
Ce	85.9	67.1	128	82.9	96.9	57.4	94.9	108	153
Pr	8.76	7.44	12.6	8.18	9.01	6.38	9.79	10.7	16.7
Nd	28.8	27.6	39.9	26.0	27.0	24.6	32.2	35.1	57.0
Sm	4.97	5.76	6.07	4.17	4.52	5.01	5.51	5.82	10.0
Eu	0.946	1.56	0.897	0.720	0.574	1.47	1.02	0.916	1.64
Gd	3.88	5.50	4.14	3.12	3.20	4.93	4.20	4.19	7.83
Tb	0.61	0.93	0.61	0.51	0.60	0.86	0.65	0.66	1.30
Dy	3.27	5.28	3.24	2.96	3.45	4.94	3.47	3.35	7.14
Ho	0.62	1.07	0.61	0.59	0.71	0.97	0.65	0.62	1.34
Er	1.87	3.22	1.83	1.84	2.34	2.93	1.92	1.92	4.15
Tm	0.282	0.478	0.291	0.291	0.398	0.433	0.290	0.286	0.636
Yb	1.83	2.99	1.90	1.91	2.62	2.77	1.81	1.82	3.80
Lu	0.268	0.413	0.271	0.281	0.370	0.395	0.264	0.251	0.460

Sample	MI-2	Dioritez	BGZ	BCOZ	101Z	BWEN	LGZ	BC101Z	BW32
Longitude	114.6927	114.6676	114.6788	114.7120	114.6280	114.6670	114.7461	114.7139	114.6542
Latitude	35.1225	35.1788	35.1705	35.2002	35.2269	35.2412	35.2594	35.1996	35.1663
Rock type	MG	diorite	FGG	SMG	SMG	enclave	SM LG	SMG	SM QM
SiO2	74.01	53.56	73.83	72.33	69.93	58.15	76.80	70.84	64.38
Al2O3	13.79	17.02	14.23	14.62	15.18	19.54	12.65	14.77	18.69
Fe2O3	1.98	7.80	1.56	2.06	2.65	5.23	0.92	2.37	2.46
MnO	0.04	0.13	0.04	0.04	0.05	0.11	0.05	0.06	0.05
MgO	0.56	6.77	0.34	0.50	0.77	1.66	0.10	0.69	0.44
CaO	1.59	8.76	1.48	1.62	1.41	3.29	0.67	1.71	1.53
Na2O	3.31	3.62	3.63	3.65	4.42	5.87	3.92	4.06	4.75
K2O	4.37	1.22	4.62	4.78	4.91	4.71	4.75	4.95	7.13
TiO2	0.27	0.95	0.23	0.29	0.52	0.98	0.13	0.43	0.49
P2O5	0.09	0.17	0.05	0.09	0.14	0.45	0.02	0.13	0.09
Rb	141	46	169	159	84	84	236	131	96
Sr	215	386	243	311	323	507	27	272	383
Ba	822	337	1009	1212	1085	1805	92	886	1932
Cs	0.8	0.4	0.8	0.7	0.2	0.3	0.7	1.0	0.4
Ta	1.21	0.50	0.84	1.37	1.03	0.52	3.33	1.74	0.59
Nb	16.2	8.2	15.3	14.1	21.3	21.8	38.3	24.3	11.1
Tl	0.74	0.30	0.63	0.91	0.44	0.47	0.86	0.82	0.53
Pb	20	9	30	28	18	19	28	24	25
Hf	4.5	3.4	4.4	5.0	8.2	19.2	4.1	5.8	10.4
Zr	163	137	150	186	322	907	83	229	421
Y	23	21	19	16	26	31	18	28	19
Sc	4.8	27.1	3.2	3.5	4.2	6.6	1.8	3.9	3.5
Cr	5.9	165	<0.5	3.3	2.6	<0.8	<0.5	1.7	<0.7
Ni	5	4	<1	2	2	1	<1	2	<1
V	20	137	15	23	31	74	5	29	22
Cu	4	12	4	3	3	7	1	4	<1
Th	14.9	4.04	14.8	12.1	7.72	6.77	19.1	17.4	12.5
U	2.03	0.67	1.14	1.43	0.84	0.53	2.67	1.81	0.55
Ga	18	27	27	27	26	35	31	28	31
La	54.0	31.6	54.1	66.5	95.8	162	46.7	106	183
Ce	99.9	61.0	101	123	181	287	77.7	187	336
Pr	10.3	6.32	9.75	11.5	17.4	27.6	6.39	17.8	33.6
Nd	34.1	25.3	34.5	40.6	62.0	95.2	17.9	60.0	115
Sm	5.78	5.09	6.07	6.04	10.1	13.5	2.76	9.41	15.8
Eu	0.896	1.53	1.04	1.12	1.74	2.88	0.235	1.52	2.45
Gd	4.37	4.69	4.35	4.02	7.14	9.61	2.16	7.06	9.76
Tb	0.71	0.85	0.75	0.63	1.16	1.40	0.43	1.18	1.23
Dy	3.78	4.53	3.86	3.16	5.83	6.82	2.60	5.98	5.14
Ho	0.74	0.89	0.78	0.59	1.10	1.27	0.58	1.16	0.87
Er	2.25	2.85	2.46	1.91	3.35	3.77	2.18	3.64	2.55
Tm	0.338	0.400	0.372	0.289	0.457	0.520	0.400	0.534	0.348
Yb	2.20	2.46	2.29	1.71	2.61	3.20	2.67	3.06	2.06
Lu	0.314	0.334	0.337	0.251	0.342	0.466	0.404	0.393	0.308

Sample	SWZ	BW24	BW41	BW47	BW36	BW33	BD3	BD9	BD16
Longitude	114.6655	114.6919	114.7107	114.7102	114.7208	114.6571	114.7133	114.7282	114.6810
Latitude	35.2400	35.2651	35.2004	35.1929	35.1992	35.1665	35.1806	35.2045	35.2076
Rock type	SM QM	SM LG	SMG	SM LG	SMG	FGG	dike	dike	dike
SiO2	63.19	77.74	67.55	77.01	73.59	70.93	72.67	72.42	71.50
Al2O3	17.64	12.14	16.22	13.24	14.27	15.00	14.51	14.39	14.36
Fe2O3	4.10	0.93	3.73	0.52	1.35	2.47	2.01	2.08	2.49
MnO	0.09	0.02	0.06	0.03	0.04	0.05	0.04	0.04	0.04
MgO	1.35	0.11	1.14	0.04	0.32	0.63	0.63	0.53	0.86
CaO	2.73	0.65	3.24	0.72	1.10	2.00	1.78	1.68	2.12
Na2O	4.70	2.86	4.00	4.32	3.90	3.59	3.49	3.64	3.62
K2O	5.07	5.35	3.36	4.03	5.14	4.82	4.52	4.79	4.53
TiO2	0.87	0.16	0.53	0.06	0.23	0.38	0.27	0.33	0.36
P2O5	0.27	0.02	0.16	0.03	0.06	0.11	0.09	0.08	0.10
Rb	83	80	97	196	133	125	155	155	125
Sr	551	83	456	11	188	315	287	209	271
Ba	1850	253	1103	17	699	1291	980	956	1099
Cs	0.3	0.4	2.0	1.0	0.9	0.9	1.2	1.4	1.0
Ta	1.11	0.51	0.98	0.60	1.53	1.33	1.05	1.56	0.93
Nb	19.2	7.0	13.7	10.7	18.7	16.1	12.3	17.6	12.0
Tl	0.38	0.48	0.71	1.34	0.87	0.59	1.04	0.93	0.63
Pb	21	21	16	35	24	23	26	19	26
Hf	12.3	4.5	5.6	2.2	3.9	5.0	4.2	5.4	4.4
Zr	557	152	204	47	125	186	140	192	175
Y	26	14	20	5	18	24	15	21	16
Sc	7.0	2.1	7.5	2.5	2.6	4.1	3.9	4.2	5.7
Cr	<0.7	1.5	3.6	1.4	<0.6	2.6	<0.5	2.0	8.1
Ni	4	<1	2	<1	<1	2	3	8	8
V	57	5	56	<5	11	21	20	21	36
Cu	5	3	8	1	2	5	20	12	8
Th	8.91	4.41	9.14	20.9	19.2	11.7	13.8	19.1	12.4
U	1.09	0.43	1.41	3.02	2.88	0.79	1.91	2.60	1.67
Ga	22	14	20	18	18	17	18	18	25
La	103	28.0	53.2	12.3	65.1	58.3	42.2	60.9	44.3
Ce	210	57.1	102	22.8	114	108	77.3	111	80.6
Pr	21.7	5.95	10.2	1.88	10.1	10.5	7.54	10.5	7.77
Nd	79.5	21.9	38.5	5.37	33.0	38.7	27.2	36.9	28.1
Sm	12.0	4.05	6.61	0.73	5.01	6.61	4.68	6.06	4.66
Eu	2.41	0.958	1.46	0.113	0.807	1.28	0.871	1.07	0.931
Gd	7.86	3.15	5.07	0.50	3.62	5.11	3.49	4.50	3.40
Tb	1.15	0.55	0.83	0.09	0.63	0.87	0.57	0.75	0.56
Dy	5.65	3.01	4.03	0.52	3.34	4.60	2.89	3.85	2.85
Ho	1.00	0.56	0.77	0.13	0.67	0.90	0.54	0.72	0.53
Er	3.06	1.74	2.43	0.59	2.14	2.80	1.72	2.36	1.74
Tm	0.442	0.257	0.339	0.119	0.308	0.400	0.255	0.350	0.263
Yb	2.92	1.60	2.14	0.92	2.05	2.51	1.58	2.30	1.65
Lu	0.414	0.233	0.294	0.168	0.294	0.341	0.233	0.328	0.230

Sample	BD18	BD24	BD35	BD39	MD3	MD9	SML47	SML49Z	SML52
Longitude	114.6886	114.6878	114.7075	114.6887	114.6769	114.6928	114.7925	114.7869	114.7833
Latitude	35.2127	35.2025	35.1798	35.1804	35.1864	35.2028	35.1320	35.1364	35.1346
Rock type	dike	dike	dike	dike	dike	Dike	SM LG	SM LG	SM LG
SiO2	73.21	69.17	73.12	72.44	53.44	58.65	77.31	77.37	77.00
Al2O3	14.25	15.45	14.20	14.42	16.93	16.11	12.28	12.46	12.50
Fe2O3	1.91	2.95	1.93	2.10	8.20	7.13	0.85	0.68	0.99
MnO	0.04	0.05	0.04	0.04	0.12	0.11	0.03	0.05	0.06
MgO	0.52	0.93	0.48	0.59	5.29	4.62	0.13	0.09	0.13
CaO	1.56	2.80	1.59	2.06	7.33	6.61	0.55	0.43	0.48
Na2O	3.48	3.87	3.57	3.57	4.06	3.45	3.44	4.08	4.04
K2O	4.68	4.18	4.72	4.38	2.18	2.03	5.22	4.69	4.62
TiO2	0.27	0.44	0.27	0.30	1.70	1.11	0.14	0.12	0.16
P2O5	0.08	0.14	0.08	0.10	0.74	0.18	0.04	0.04	0.02
Rb	144	105	147	132	38	47	159	204	154
Sr	225	384	246	235	1167	351	73	17	42
Ba	796	1407	848	685	1409	568	277	37	120
Cs	0.7	0.6	1.1	0.7	0.3	0.4	1	0.7	0.7
Ta	1.17	0.83	1.18	1.19	1.32	0.85	1.5	3.2	2.3
Nb	13.5	11.1	13.3	15.6	24.1	11.8	20	43.8	30.8
Tl	1.04	0.47	0.75	0.68	0.23	0.28	0.7	0.88	0.79
Pb	27	23	26	27	10	8	24	31	13
Hf	4.6	4.5	4.3	4.8	8.0	4.1	2.8	4.2	4.6
Zr	159	163	139	169	326	149	83	99	137
Y	16	17	16	18	24	23	20	19	27
Sc	3.8	6.1	4.1	4.5	17.5	21.1	1.05	1.31	1.18
Cr	<0.6	5.3	8.2	3.1	72.6	85.2	< 0.5	< 0.5	< 0.5
Ni	3	5	3	3	67	57	1	1	< 1
V	21	44	19	23	172	134	7	< 5	5
Cu	6	3	6	10	69	27	6	11	6
Th	15.8	9.86	14.9	15.0	8.51	6.83	10.9	20.8	17
U	1.88	1.40	2.14	2.15	1.57	1.03	1.58	2.89	1.87
Ga	17	18	18	18	23	18	17	20	20
La	49.3	46.8	42.5	44.1	99.3	33.2	39.9	36	40.6
Ce	89.6	86.5	79.3	81.6	190	65.2	76	63	87.4
Pr	8.56	8.37	7.70	8.01	19.6	6.74	8.03	5.77	8.29
Nd	30.4	31.0	27.5	29.6	74.7	26.2	25.1	15.7	25.9
Sm	5.04	5.26	4.65	5.11	11.6	5.12	4.42	2.49	4.56
Eu	0.851	1.17	0.841	0.933	3.04	1.40	0.581	0.202	0.414
Gd	3.63	3.92	3.50	4.08	8.03	4.61	3.14	1.65	3.16
Tb	0.58	0.65	0.59	0.67	1.10	0.82	0.62	0.38	0.64
Dy	2.95	3.32	3.05	3.49	5.34	4.48	3.49	2.48	4.09
Ho	0.54	0.65	0.58	0.65	0.91	0.89	0.69	0.58	0.88
Er	1.75	1.99	1.93	2.10	2.79	2.88	2.21	2.15	2.9
Tm	0.280	0.291	0.286	0.320	0.373	0.427	0.328	0.387	0.466
Yb	1.77	1.80	1.85	1.97	2.40	2.63	1.97	2.62	2.86
Lu	0.253	0.251	0.275	0.294	0.332	0.370	0.257	0.395	0.384

Sample	SML54Z	SML59Z	SML63C	SML67	SML69	SML71	SML73
Longitude	114.7428	114.7269	114.7476	114.7462	114.7522	114.7579	114.7604
Latitude	35.1817	35.2559	35.2584	35.2575	35.1796	35.1819	35.1806
Rock type	SM	roof unit	SM LG	SM LG	SM LG	SM LG	SM LG
SiO2	75.57	74.41	77.19	78.49	77.96	78.10	77.84
Al2O3	13.09	13.82	12.03	12.12	12.22	11.92	12.11
Fe2O3	1.19	1.11	1.46	0.67	0.57	0.81	0.77
MnO	0.05	0.06	0.07	0.01	0.04	0.05	0.07
MgO	0.28	0.15	0.11	0.04	0.07	0.07	0.07
CaO	0.78	0.42	0.24	0.38	0.43	0.40	0.33
Na2O	3.67	4.34	3.62	3.94	3.94	3.90	3.87
K2O	5.12	5.45	5.05	4.23	4.68	4.58	4.79
TiO2	0.20	0.21	0.21	0.10	0.09	0.13	0.12
P2O5	0.05	0.03	0.02	0.01	0.01	0.03	0.02
Rb	157	148	184	143	177	189	277
Sr	89	63	4	5	23	12	15
Ba	326	252	22	10	59	37	49
Cs	0.8	0.9	1.1	0.3	0.7	0.7	1.4
Ta	1.5	2	4.7	3.7	1.8	3.1	3.6
Nb	23.4	31.2	65.3	49.8	21.9	44.3	60.7
Tl	0.82	0.68	0.73	0.63	0.71	0.92	1.5
Pb	30	19	24	20	28	33	43
Hf	4.2	6.6	8.1	5.6	2.9	5.4	6.2
Zr	127	199	186	114	68	131	128
Y	16	26	42	20	15	23	22
Sc	1.97	1.7	1.84	2.03	0.91	1.18	2.15
Cr	< 0.5	< 0.5	< 0.5	< 0.5	< 0.5	< 0.5	< 0.5
Ni	3	< 1	2	< 1	< 1	< 1	2
V	11	7	< 5	< 5	< 5	< 5	< 5
Cu	7	6	6	27	18	9	7
Th	17.1	15.3	44.3	38.5	17.5	25.3	67.7
U	1.34	1.79	2.99	4.71	2.14	4.01	8.12
Ga	18	19	22	21	18	18	19
La	36.5	62	60.5	41.8	32.7	43.9	38.9
Ce	73.2	120	123	64.8	59.9	77.3	65.3
Pr	7.81	12.7	12	5.48	5.64	7.01	5.6
Nd	23.7	37.5	35.1	13.6	15.8	18.8	14.6
Sm	3.93	6.53	5.91	1.84	2.66	2.84	2.2
Eu	0.546	0.777	0.197	0.09	0.229	0.203	0.157
Gd	2.52	4.37	4.43	1.08	1.69	1.84	1.49
Tb	0.47	0.76	0.97	0.28	0.36	0.4	0.34
Dy	2.61	4.14	6.3	2.05	2.32	2.72	2.43
Ho	0.55	0.84	1.41	0.51	0.51	0.65	0.61
Er	1.81	2.69	4.82	2.01	1.74	2.43	2.43
Tm	0.298	0.41	0.8	0.404	0.294	0.445	0.455
Yb	1.89	2.52	5	3.02	1.89	3.09	3.35
Lu	0.272	0.359	0.684	0.493	0.268	0.481	0.544

Sample	SML74	SML76	SML78	MPL53Z	MI-1
Longitude	114.7628	114.7671	114.7719	114.6926	114.6782
Latitude	35.1806	35.1826	35.1812	35.1225	35.1312
Rock type	SM LG	SM LG	SM LG	MG	MG
SiO2	77.55	77.51	78.59	73.77	73.69
Al2O3	12.30	12.40	11.97	13.82	13.66
Fe2O3	0.73	0.73	0.59	1.86	2.19
MnO	0.07	0.09	0.08	0.04	0.04
MgO	0.07	0.05	0.03	0.54	0.61
CaO	0.40	0.35	0.20	1.56	1.85
Na2O	3.94	4.31	4.19	3.39	3.28
K2O	4.80	4.50	4.26	4.72	4.25
TiO2	0.12	0.07	0.08	0.24	0.32
P2O5	0.01	0.00	0.01	0.07	0.09
Rb	284	321	286	150	124
Sr	13	7	5	200	261
Ba	48	20	19	830	915
Cs	3.1	3.5	1.9	0.8	0.7
Ta	3.8	3.8	3.7	1.2	1.48
Nb	51.9	50.2	55.4	16.9	14.2
Tl	1.29	1.6	1.49	0.85	0.71
Pb	28	41	36	33	21
Hf	5.2	6.9	5.4	4.9	5.6
Zr	111	123	96	166	203
Y	23	24	18	22	23
Sc	1.79	1.79	1.6	4.22	4.9
Cr	< 0.5	< 0.5	< 0.5	6.6	8.6
Ni	< 1	2	1	3	5
V	< 5	< 5	< 5	18	25
Cu	8	8	6	7	3
Th	29.8	41.5	33.6	15.8	18.7
U	3.06	6.27	4.88	2.33	2.13
Ga	20	24	22	17	18
La	50.6	44.6	26.7	53.5	58.9
Ce	86.1	74.2	49.6	99.5	110
Pr	7.38	5.81	4.41	10.8	11.2
Nd	18.8	14.1	11.9	33	36.6
Sm	2.76	1.94	1.79	5.62	6.20
Eu	0.174	0.103	0.076	0.913	1.06
Gd	1.59	1.17	1.33	3.82	4.82
Tb	0.38	0.31	0.28	0.69	0.75
Dy	2.55	2.32	2.1	3.57	4.09
Ho	0.64	0.6	0.51	0.71	0.77
Er	2.4	2.39	1.96	2.3	2.34
Tm	0.448	0.475	0.37	0.353	0.351
Yb	3.18	3.73	2.66	2.24	2.25
Lu	0.507	0.588	0.421	0.343	0.312

APPENDIX D

TABULATED GEOCHRONOLOGY DATA

Spot Name	% comm 206	ppm U	ppm Th	232Th /238U	207corr 206Pb /238U Age	1σ err	7corr 206Pbr /238U	1σ err	Total 238 /206	% err	Total 207 /206	% err
BD18-1.1	0.02	2696.58	1023.17	0.39	169.99	0.44	0.02672	0.000069	37.42	0.25	0.05	0.89
BD18-2.1	1.07	159.91	36.32	0.23	15.73	0.40	0.00244	0.000063	404.94	2.44	0.05	11.00
BD18-2.2	-1.48	60.37	86.81	1.49	16.00	0.73	0.00249	0.000114	408.31	4.31	0.03	36.12
BD18=3.1	0.30	484.01	1820.43	3.89	15.71	0.88	0.00244	0.000137	408.67	5.60	0.05	8.72
BD18-4.1	-0.16	308.74	231.24	0.77	16.39	0.35	0.00254	0.000055	393.56	2.07	0.05	11.25
BD18-4.2	1.08	39.49	56.15	1.47	71.45	2.16	0.01115	0.000339	88.76	2.90	0.06	12.42
BD18-5.1	11.33	1401.69	3036.03	2.24	15.62	0.17	0.00243	0.000026	365.46	0.90	0.14	2.79
BD18-6.1	0.68	222.34	414.99	1.93	17.04	0.38	0.00265	0.000060	375.22	2.14	0.05	10.92
BD18-7.1	0.12	521.82	518.62	1.03	16.22	0.26	0.00252	0.000040	396.52	1.53	0.05	7.83
BD18-8.1	0.54	494.81	2235.56	4.67	15.34	0.25	0.00238	0.000040	417.38	1.58	0.05	7.86
BD18-9.1	-0.21	534.39	1650.99	3.19	16.19	0.27	0.00251	0.000042	398.50	1.60	0.04	8.74
BD18-10.1	0.41	380.53	444.24	1.21	15.44	0.28	0.00240	0.000043	415.34	1.71	0.05	8.39
BD18-11.1	-0.08	202.14	85.68	0.44	101.72	1.18	0.01590	0.000186	62.93	1.13	0.05	4.95
BD18-12.1	-0.13	173.24	116.44	0.69	98.49	1.15	0.01540	0.000181	65.04	1.13	0.05	5.10
BD18-13.1	2.37	112.58	128.12	1.18	17.17	0.56	0.00267	0.000087	365.96	3.04	0.07	14.28
BD18-8.2	1.10	194.97	102.92	0.55	15.05	0.38	0.00234	0.000059	423.07	2.36	0.05	12.07
BD18-7.2	-0.28	401.77	408.57	1.05	16.17	0.28	0.00251	0.000043	399.34	1.65	0.04	8.94
BD18-14.1	-0.21	140.40	84.29	0.62	14.93	0.46	0.00232	0.000072	432.11	2.91	0.04	18.27
BD35-1.1	0.44	104.74	198.58	1.96	17.51	0.61	0.00272	0.000095	366.04	3.28	0.05	18.45
BD35-2.1	0.34	594.49	1525.99	2.65	16.07	0.24	0.00250	0.000037	399.37	1.43	0.05	6.99
BD35-3.1	-0.94	40.62	65.12	1.66	16.43	1.01	0.00255	0.000157	395.53	5.81	0.04	42.39
BD35-4.1	0.05	103.01	120.39	1.21	17.46	0.53	0.00271	0.000082	368.60	2.85	0.05	17.36
BD35-5.1	0.93	523.99	462.88	0.91	15.74	0.22	0.00244	0.000035	405.21	1.33	0.05	7.27
BD35-6.1	0.57	198.33	268.54	1.40	16.38	0.37	0.00254	0.000058	390.78	2.17	0.05	11.48
BD35-7.1	0.71	228.76	143.24	0.65	16.73	0.64	0.00260	0.000099	382.15	3.70	0.05	13.04
BD35-8.1	-0.17	695.33	1611.43	2.39	15.92	0.20	0.00247	0.000032	405.05	1.22	0.04	6.62
BD35-9.1	-0.35	378.09	1277.76	3.49	15.69	0.27	0.00244	0.000042	411.87	1.63	0.04	9.61
BD35-10.1	0.20	710.41	1457.98	2.12	15.23	0.19	0.00237	0.000029	421.86	1.17	0.05	6.15
BD35-11.1	-0.13	1051.41	3390.50	3.33	15.33	0.16	0.00238	0.000024	420.66	0.97	0.05	5.43

Spot Name	% comm 206	ppm U	ppm Th	232Th /238U	207corr 206Pb /238U Age	1σ err	7corr 206Pbr /238U	1σ err	Total 238 /206	% err	Total 207 /206	% err
BD35-12.1	1.59	319.40	279.63	0.90	14.24	0.30	0.00221	0.000046	444.91	1.98	0.06	8.62
BD35-13.1	0.92	343.84	446.82	1.34	16.05	0.27	0.00249	0.000042	397.40	1.60	0.05	8.17
BD35-14.1	9.54	298.95	343.60	1.19	15.04	0.29	0.00234	0.000045	387.21	1.67	0.12	5.73
BD35-15.1	-0.05	488.66	565.22	1.20	14.80	0.21	0.00230	0.000032	435.37	1.33	0.05	7.42
BD35-16.1	0.21	396.58	392.07	1.02	14.85	0.23	0.00231	0.000037	432.78	1.50	0.05	8.11
BD35-17.1	0.64	537.66	375.26	0.72	15.92	0.22	0.00247	0.000035	401.73	1.33	0.05	6.84
BD35-18.1	0.71	407.00	455.85	1.16	15.50	0.25	0.00241	0.000038	412.52	1.51	0.05	7.78
BC101Z-1.1	2.06	227.93	263.24	1.19	16.29	0.35	0.00253	0.000055	387.04	2.02	0.06	9.57
BC101Z-2.1	-0.76	63.26	131.32	2.15	16.79	0.69	0.00261	0.000107	386.42	3.88	0.04	26.88
BC101Z-2.2	1.32	81.68	100.73	1.27	14.79	0.58	0.00230	0.000090	429.57	3.64	0.06	19.78
BC101Z-3.1	1.48	179.16	198.47	1.14	16.03	0.38	0.00249	0.000059	395.77	2.24	0.06	10.20
BC101Z-4.1	0.72	681.40	955.92	1.45	16.53	0.20	0.00257	0.000031	386.77	1.15	0.05	5.73
BC101Z-5.1	-0.32	139.47	168.64	1.25	17.01	0.44	0.00264	0.000069	379.61	2.44	0.04	16.54
BC101Z-6.1	1.19	336.85	433.01	1.33	16.26	0.28	0.00253	0.000044	391.24	1.64	0.06	8.15
BC101Z-7.1	0.28	243.45	393.44	1.67	16.74	0.34	0.00260	0.000053	383.53	1.92	0.05	10.38
BC101Z-8.1	-0.27	302.93	379.36	1.29	16.50	0.29	0.00256	0.000045	391.14	1.66	0.04	9.94
BC101Z-9.1	0.62	1531.52	1689.87	1.14	16.61	0.13	0.00258	0.000021	385.18	0.77	0.05	3.84
BC101Z-10.1	0.46	231.01	740.25	3.31	16.57	0.38	0.00257	0.000058	386.69	2.18	0.05	10.12
BC101Z-11.1	0.54	221.97	258.00	1.20	15.67	0.34	0.00243	0.000053	408.70	2.03	0.05	11.20
BC101Z-11.12	0.20	891.04	1154.05	1.34	16.78	0.17	0.00261	0.000027	382.82	0.99	0.05	5.10
BC101Z-12.1	0.80	292.71	393.00	1.39	16.28	0.30	0.00253	0.000046	392.42	1.73	0.05	9.31
BC101Z-13.1	-2.31	102.92	199.14	2.00	15.13	0.50	0.00235	0.000077	435.31	3.09	0.03	31.86
BC101Z-14.1	2.27	115.50	194.93	1.74	15.33	0.50	0.00238	0.000078	410.46	3.09	0.06	13.18
BC101Z-14.2	1.25	259.75	369.52	1.47	15.57	0.30	0.00242	0.000047	408.47	1.81	0.06	8.89
BC101Z-18.1	-0.47	749.05	1154.34	1.59	15.43	0.18	0.00240	0.000027	419.12	1.09	0.04	6.25
BC101Z-19.1	0.23	379.70	593.24	1.61	16.27	0.27	0.00253	0.000042	394.70	1.51	0.05	10.95
SWZ-1.1	4.11	80.02	137.97	1.78	15.05	0.54	0.00234	0.000085	410.16	3.26	0.08	15.09
SWZ-1.2	1.52	84.48	171.68	2.10	14.85	0.57	0.00231	0.000089	427.08	3.61	0.06	18.41
SWZ-2.1	1.48	294.01	317.75	1.12	15.65	0.29	0.00243	0.000045	405.33	1.74	0.06	8.52

Spot Name	% comm 206	ppm U	ppm Th	232Th /238U	207corr 206Pb /238U Age	1σ err	7corr 206Pbr /238U	1σ err	Total 238 /206	% err	Total 207 /206	% err
SWZ-3.1	0.95	123.91	124.86	1.04	16.02	0.45	0.00249	0.000070	398.08	2.65	0.05	14.20
SWZ-4.1	0.80	639.77	1205.59	1.95	15.63	0.19	0.00243	0.000030	408.60	1.17	0.05	5.97
SWZ-5.1	0.24	184.23	262.82	1.47	16.74	0.38	0.00260	0.000059	383.70	2.12	0.05	12.63
SWZ-5.2	0.09	80.13	149.34	1.93	15.53	0.57	0.00241	0.000088	414.19	3.41	0.05	22.18
SWZ-3.2	0.76	191.87	394.17	2.12	17.44	0.55	0.00271	0.000085	366.30	3.05	0.05	11.74
SWZ-6.1	-0.70	180.75	295.07	1.69	16.49	0.46	0.00256	0.000071	393.25	2.66	0.04	14.92
SWZ-7.1	-0.19	309.52	870.77	2.91	16.58	0.29	0.00258	0.000046	389.00	1.70	0.04	9.25
SWZ-7.2	1.10	139.00	272.11	2.02	16.53	0.44	0.00257	0.000068	385.08	2.50	0.06	13.09
SWZ-8.1	2.18	146.88	195.98	1.38	16.16	0.44	0.00251	0.000068	389.81	2.52	0.06	11.98
SWZ-9.1	0.48	524.44	860.39	1.70	15.64	0.22	0.00243	0.000034	409.71	1.34	0.05	6.78
SWZ-10.1	1.00	141.87	148.58	1.08	16.82	0.45	0.00261	0.000070	378.99	2.52	0.05	13.13
SWZ-11.1	0.19	233.26	768.73	3.41	16.27	0.35	0.00253	0.000054	395.01	2.00	0.05	11.87
SWZ-12.1	0.70	106.37	247.09	2.40	15.38	0.48	0.00239	0.000075	415.61	2.95	0.05	16.95
SWZ-13.1	1.04	131.53	239.21	1.88	16.71	0.46	0.00259	0.000071	381.35	2.58	0.05	13.61
SWZ-14.1	1.99	70.22	144.42	2.12	16.12	0.58	0.00250	0.000091	391.51	3.41	0.06	15.27
SWZ-15.1	3.31	151.54	307.61	2.10	15.73	0.40	0.00244	0.000063	395.83	2.36	0.07	10.60
SWZ-15.2	5.27	63.60	221.02	3.59	15.80	0.65	0.00245	0.000101	385.94	3.69	0.09	15.61
SWZ-16.1	4.18	51.54	88.63	1.78	14.28	0.65	0.00222	0.000101	431.93	4.16	0.08	17.03
SWZ-16.2	0.10	867.22	1193.36	1.42	15.98	0.16	0.00248	0.000026	402.36	0.98	0.05	5.32
SWZ-17.1	3.05	1069.20	1686.36	1.63	16.97	0.17	0.00264	0.000027	367.75	0.86	0.07	5.66
SWZ-17.2	3.61	52.81	67.38	1.32	15.63	0.72	0.00243	0.000112	397.08	4.11	0.07	21.44
DSCG-1.1	-1.17	127.13	164.67	1.34	15.62	0.43	0.00243	0.000068	416.87	2.62	0.04	19.80
DSCG-2.1	0.48	601.00	850.70	1.46	16.63	0.21	0.00258	0.000032	385.35	1.19	0.05	6.15
DSCG-2.2	0.36	249.29	304.00	1.26	16.65	0.33	0.00259	0.000051	385.29	1.88	0.05	10.57
DSCG-3.1	3.08	52.83	158.73	3.10	15.98	0.72	0.00248	0.000113	390.50	4.14	0.07	20.01
DSCG-4.1	0.72	264.81	340.15	1.33	15.99	0.31	0.00248	0.000047	399.73	1.81	0.05	9.10
DSCG-5.1	1.56	44.79	146.09	3.37	16.18	0.81	0.00251	0.000125	391.80	4.56	0.06	26.48
DSCG-6.1	0.43	67.41	234.33	3.59	15.83	0.62	0.00246	0.000096	404.91	3.63	0.05	22.87
DSCG-6.2	1.69	321.30	499.49	1.61	15.51	0.27	0.00241	0.000042	407.99	1.64	0.06	7.79

Spot Name	% comm 206	ppm U	ppm Th	232Th /238U	207corr 206Pb /238U Age	1σ err	7corr 206Pbr /238U	1σ err	Total 238 /206	% err	Total 207 /206	% err
DSCG-7.1	-0.49	306.11	397.74	1.34	16.10	0.29	0.00250	0.000045	401.80	1.70	0.04	9.84
DSCG-8.1	4.01	195.36	221.79	1.17	15.37	0.35	0.00239	0.000055	402.08	2.12	0.08	8.48
DSCG-9.1	0.27	1045.81	1458.52	1.44	16.19	0.31	0.00251	0.000048	396.72	1.87	0.05	4.81
DSCG-9.2	0.77	238.26	285.84	1.24	15.67	0.31	0.00243	0.000049	407.78	1.94	0.05	7.67
DSCG-10.1	1.72	402.21	424.11	1.09	15.70	0.24	0.00244	0.000038	403.11	1.47	0.06	6.93
DSCG-10.2	0.67	2230.02	4776.24	2.21	17.96	0.12	0.00279	0.000019	356.13	0.67	0.05	2.91
DSCG-10.3	-0.02	2080.55	3203.79	1.59	16.56	0.11	0.00257	0.000017	388.81	0.63	0.05	3.22
DSCG-11.2	2.80	88.13	121.35	1.42	16.19	0.56	0.00251	0.000086	386.66	3.16	0.07	15.02
DSCG-12.1	0.27	4477.87	15767.83	3.64	15.71	0.07	0.00244	0.000011	408.67	0.45	0.05	2.27
DSCG-12.2	-0.23	156.00	226.65	1.50	15.63	0.41	0.00243	0.000063	412.94	2.46	0.04	14.94
DSCG-13.1	0.54	6136.51	15642.22	2.63	17.73	0.07	0.00275	0.000011	361.17	0.38	0.05	1.89
DSCG-13.2	-1.70	41.64	70.15	1.74	14.55	0.77	0.00226	0.000120	450.10	4.94	0.03	48.81
DSCG-14.1	0.27	1713.00	3155.12	1.90	16.20	0.12	0.00252	0.000019	396.35	0.70	0.05	3.58
DSCG-14.2	2.04	709.07	1645.87	2.40	14.73	0.18	0.00229	0.000028	428.19	1.13	0.06	6.07
LGZ-1.1	2.68	55.08	125.07	2.35	16.23	0.80	0.00252	0.000125	385.95	4.46	0.07	23.78
LGZ-2.1	0.59	1531.44	3381.85	2.28	17.85	0.15	0.00277	0.000024	358.51	0.81	0.05	3.95
LGZ-2.2	0.49	1366.81	1513.75	1.14	16.67	0.16	0.00259	0.000025	384.34	0.93	0.05	4.53
LGZ-3.1	1.30	73.49	140.30	1.97	16.61	0.67	0.00258	0.000104	382.64	3.74	0.06	20.59
LGZ-3.2	5.19	1978.84	2872.51	1.50	17.57	0.19	0.00273	0.000029	347.33	0.75	0.09	2.81
LGZ-4.1	1.00	280.76	356.67	1.31	16.91	0.35	0.00263	0.000055	376.83	1.96	0.05	9.65
LGZ-5.1	0.61	562.13	706.10	1.30	16.82	0.25	0.00261	0.000039	380.38	1.42	0.05	7.00
LGZ-6.1	0.32	724.76	1240.99	1.77	16.45	0.21	0.00256	0.000033	390.09	1.24	0.05	6.29
LGZ-7.1	0.12	2446.11	4970.69	2.10	17.73	0.12	0.00275	0.000019	362.55	0.65	0.05	3.24
LGZ-8.1	-0.23	77.69	114.54	1.52	16.33	0.71	0.00254	0.000110	395.28	4.15	0.04	23.23
LGZ-9.1	1.14	288.54	359.78	1.29	16.72	0.32	0.00260	0.000050	380.69	1.81	0.06	8.62
LGZ-10.1	-0.11	704.99	806.32	1.18	17.32	0.22	0.00269	0.000034	372.04	1.21	0.05	6.64
LGZ-10.2	-0.24	160.01	631.80	4.08	17.44	0.49	0.00271	0.000076	370.07	2.65	0.04	16.00
LGZ-11.1	22.55	37.97	127.35	3.47	15.85	1.19	0.00246	0.000184	314.66	4.80	0.22	12.01
LGZ-11.2	0.93	728.06	731.49	1.04	16.21	0.21	0.00252	0.000033	393.48	1.23	0.05	5.83

Spot Name	% comm 206	ppm U	ppm Th	232Th /238U	207corr 206Pb /238U Age	1σ err	7corr 206Pbr /238U	1σ err	Total 238 /206	% err	Total 207 /206	% err
LGZ-12.1	0.22	314.62	919.88	3.02	16.71	0.31	0.00260	0.000048	384.31	1.75	0.05	9.01
LGZ-13.1	1.21	42.93	106.37	2.56	17.35	0.92	0.00270	0.000143	366.52	4.85	0.06	29.30
LGZ-14.1	-0.05	5285.03	9487.34	1.85	17.81	0.08	0.00277	0.000012	361.74	0.43	0.05	2.30
LGZ-15.1	0.18	672.06	809.89	1.25	17.36	0.22	0.00270	0.000034	370.10	1.20	0.05	6.24
LGZ-16.1	2.03	607.34	731.90	1.25	17.04	0.30	0.00265	0.000046	370.10	1.20	0.06	15.32
LGZ-16.1	0.18	1272.91	2105.65	1.71	17.42	0.16	0.00271	0.000025	369.01	0.89	0.05	4.55
LGZ-17.1	35.57	389.48	633.06	1.68	16.43	1.37	0.00255	0.000213	252.47	1.72	0.33	6.57
LGZ-18.1	0.64	1299.69	1859.97	1.48	16.84	0.15	0.00262	0.000024	379.80	0.87	0.05	4.22
dioriteZ-1.1	0.58	796.15	91.69	0.12	15.36	0.21	0.00239	0.000033	416.75	1.32	0.05	5.83
dioriteZ-2.1	-0.84	397.87	1282.63	3.33	16.59	0.30	0.00258	0.000046	391.38	1.72	0.04	10.26
dioriteZ-3.1	0.50	247.98	199.46	0.83	15.67	0.37	0.00243	0.000057	408.92	2.23	0.05	11.60
dioriteZ-4.1	-0.06	589.01	1914.04	3.36	16.62	0.25	0.00258	0.000039	387.65	1.46	0.05	7.97
dioriteZ-5.1	1.13	283.52	684.36	2.49	16.00	0.34	0.00249	0.000053	397.84	2.01	0.06	9.66
dioriteZ-1.2	0.49	784.28	74.46	0.10	15.27	0.20	0.00237	0.000032	419.59	1.27	0.05	6.28
dioriteZ-6.1	0.04	869.02	2781.39	3.31	15.56	0.19	0.00242	0.000029	413.78	1.15	0.05	5.97
dioriteZ-7.1	-0.38	237.77	97.77	0.42	15.96	0.36	0.00248	0.000056	404.88	2.16	0.04	12.41
dioriteZ-8.1	0.89	366.69	908.80	2.56	15.64	0.29	0.00243	0.000045	407.90	1.74	0.05	9.11
dioriteZ-9.1	0.02	390.77	848.03	2.24	16.14	0.29	0.00251	0.000045	398.91	1.72	0.05	9.32
dioriteZ-10.1	-0.57	185.10	427.70	2.39	15.92	0.41	0.00247	0.000064	406.75	2.48	0.04	15.44
dioriteZ-11.1	-1.19	322.50	739.88	2.37	15.92	0.36	0.00247	0.000056	409.17	2.17	0.04	13.59
dioriteZ-12.1	0.68	335.23	1063.33	3.28	14.95	0.30	0.00232	0.000047	427.79	1.92	0.05	10.35
dioriteZ-13.1	-1.25	155.34	275.21	1.83	16.09	0.45	0.00250	0.000070	405.24	2.67	0.04	17.61
dioriteZ-14.1	-0.44	169.65	371.06	2.26	15.81	0.43	0.00246	0.000066	409.01	2.57	0.04	15.11
dioriteZ-15.1	2.30	231.85	567.60	2.53	14.99	0.36	0.00233	0.000056	419.63	2.23	0.06	9.99
dioriteZ-16.1	2.01	187.18	546.25	3.02	16.73	0.43	0.00260	0.000067	377.18	2.45	0.06	9.55
dioriteZ-17.1	0.10	478.40	1213.49	2.62	16.36	0.26	0.00254	0.000041	393.08	1.52	0.05	8.05
dioriteZ-18.1	1.17	576.74	1473.55	2.64	14.67	0.34	0.00228	0.000053	433.75	2.24	0.06	7.51
dioriteZ-19.1	0.04	229.51	493.43	2.22	16.16	0.37	0.00251	0.000058	398.38	2.19	0.05	12.11
BGZ-1.1	0.36	1215.58	3610.88	3.07	15.87	0.16	0.00247	0.000025	404.15	0.98	0.05	4.95

Spot Name	% comm 206	ppm U	ppm Th	232Th /238U	207corr 206Pb /238U Age	1σ err	7corr 206Pbr /238U	1σ err	Total 238 /206	% err	Total 207 /206	% err
BGZ-2.1	0.94	212.72	290.51	1.41	16.52	0.39	0.00257	0.000061	386.11	2.25	0.05	11.44
BGZ-3.1	1.76	211.24	458.01	2.24	16.19	0.40	0.00251	0.000062	390.75	2.30	0.06	10.74
BGZ-4.1	37.71	537.81	1617.84	3.11	14.54	1.41	0.00226	0.000220	275.96	1.19	0.34	8.41
BGZ-5.1	-0.42	58.39	86.56	1.53	14.81	0.73	0.00230	0.000114	436.56	4.64	0.04	31.41
BGZ-6.1	3.14	384.89	655.90	1.76	15.89	0.31	0.00247	0.000049	392.53	1.79	0.07	7.56
BGZ-7.1	-0.34	1479.51	2725.52	1.90	16.93	0.15	0.00263	0.000023	381.56	0.85	0.04	4.68
BGZ-8.1	29.81	153.07	356.73	2.41	14.27	0.92	0.00222	0.000143	316.72	2.34	0.28	5.24
BGZ-9.1	4.53	27.74	58.58	2.18	17.52	1.21	0.00272	0.000188	350.74	6.13	0.08	28.69
BGZ-10.1	3.50	302.48	854.78	2.92	16.46	0.42	0.00256	0.000065	377.52	1.91	0.07	16.91
BGZ-11.1	2.03	135.54	300.25	2.29	16.70	0.51	0.00259	0.000079	377.66	2.83	0.06	12.89
BGZ-12.1	-0.29	288.66	574.00	2.05	17.72	0.37	0.00275	0.000057	364.44	1.98	0.04	10.67
BGZ-12.2	0.05	130.33	248.95	1.97	17.06	0.51	0.00265	0.000079	377.07	2.81	0.05	16.99
BGZ-13.1	4.28	340.09	366.78	1.11	14.94	0.34	0.00232	0.000052	412.62	1.95	0.08	9.26
BGZ-14.1	59.76	44.21	81.46	1.90	15.95	3.40	0.00248	0.000529	162.43	3.36	0.52	5.85
BGZ-15.1	1.16	363.69	782.06	2.22	15.28	0.29	0.00237	0.000045	416.41	1.79	0.06	8.54
BGZ-5.2	0.19	216.32	559.33	2.67	17.22	0.40	0.00268	0.000062	373.08	2.22	0.05	11.96
BGZ-16.1	-0.29	332.74	978.02	3.04	15.36	0.50	0.00239	0.000078	420.37	2.85	0.04	28.25
BGZ-17.1	2.26	675.94	2439.26	3.73	16.28	0.34	0.00253	0.000053	386.56	1.90	0.06	10.17
BGZ-18.1	0.52	357.80	1231.16	3.56	15.70	0.30	0.00244	0.000046	408.00	1.80	0.05	9.43
BGZ-19.1	0.80	656.65	2340.89	3.68	15.16	0.22	0.00235	0.000034	421.27	1.35	0.05	7.73
BGZ-20.1	0.77	598.10	1708.75	2.95	15.46	0.23	0.00240	0.000036	413.24	1.39	0.05	7.83
BGZ-21.1	0.35	281.31	622.12	2.29	16.50	0.34	0.00256	0.000052	388.78	1.96	0.05	9.53
101Z-1.1	3.69	35.60	84.76	2.46	16.48	1.01	0.00256	0.000157	376.24	5.49	0.08	26.96
101Z-2.1	3.97	77.51	207.84	2.77	15.07	0.64	0.00234	0.000100	410.22	3.84	0.08	17.33
101Z-3.1	-0.23	773.01	1058.96	1.42	16.79	0.21	0.00261	0.000033	384.29	1.20	0.04	6.46
101Z-4.1	5.96	189.14	497.15	2.72	17.08	0.45	0.00265	0.000071	354.36	2.29	0.09	8.72
101Z-5.1	1.46	498.79	648.44	1.34	15.74	0.41	0.00244	0.000064	403.15	2.55	0.06	6.91
101Z-5.2	1.92	92.63	202.48	2.26	16.09	0.61	0.00250	0.000094	392.56	3.52	0.06	17.19
101Z-6.1	-0.37	311.33	395.45	1.31	18.05	0.33	0.00280	0.000052	358.04	1.77	0.04	10.05

Spot Name	% comm 206	ppm U	ppm Th	232Th /238U	207corr 206Pb /238U Age	1σ err	7corr 206Pbr /238U	1σ err	Total 238 /206	% err	Total 207 /206	% err
101Z-7.1	0.53	832.14	1224.66	1.52	16.30	0.20	0.00253	0.000031	392.79	1.16	0.05	5.94
101Z-6.2	5.72	57.47	75.64	1.36	16.23	0.83	0.00252	0.000128	373.97	4.31	0.09	21.13
101Z-8.1	0.26	1528.50	2237.93	1.51	17.72	0.16	0.00275	0.000025	362.39	0.84	0.05	5.59
101Z-9.1	0.15	308.06	457.33	1.53	16.32	0.32	0.00253	0.000050	393.92	1.89	0.05	9.64
101Z-10.1	0.79	244.51	362.41	1.53	15.63	0.36	0.00243	0.000057	408.58	2.21	0.05	11.21
101Z-11.1	-0.48	213.26	232.80	1.13	17.60	0.41	0.00273	0.000063	367.57	2.21	0.04	12.99
101Z-12.1	1.33	245.48	317.13	1.33	16.50	0.38	0.00256	0.000058	385.12	2.14	0.06	10.54
101Z-13.1	0.17	523.57	664.63	1.31	17.43	0.25	0.00271	0.000039	368.70	1.37	0.05	7.18
101Z-14.1	-0.20	1035.57	1471.21	1.47	17.06	0.18	0.00265	0.000028	378.02	1.01	0.04	6.17
101Z-15.1	0.31	1657.13	2827.09	1.76	16.43	0.14	0.00255	0.000021	390.73	0.80	0.05	3.99
101Z-15.2	0.50	313.68	394.10	1.30	16.76	0.34	0.00260	0.000053	382.09	1.91	0.05	10.86
101Z-16.1	0.27	476.48	634.87	1.38	16.37	0.26	0.00254	0.000040	392.16	1.50	0.05	7.28
101Z-17.1	0.34	898.26	1613.15	1.86	16.17	0.18	0.00251	0.000028	396.73	1.08	0.05	5.37
101Z-18.1	0.75	203.54	271.18	1.38	16.30	0.40	0.00253	0.000062	392.00	2.33	0.05	12.12
101Z-19.1	1.21	75.83	256.88	3.50	15.55	0.75	0.00242	0.000117	409.00	4.53	0.06	24.23
101Z-20.1	0.55	598.71	975.98	1.68	16.99	0.23	0.00264	0.000036	376.79	1.29	0.05	6.41

REFERENCES

Anderson, J.L., Morrison, J., 2005. Ilmenite, magnetite, and peraluminous Mesoproterozoic anorogenic granites of Laurentia and Baltica. LITHOS 80 (1-4), 45-60.

Bachl, C.A., Miller, C.F., Miller, J.S., Faulds, J.E., 2001. Construction of a pluton: Evidence from an exposed cross section of the Searchlight pluton, Eldorado Mountains, Nevada. GSA Bulletin 113 (9), 1213-1228.

Bacon, C.R., Lowenstern, J.B., 2005. Late Pleistocene granodiorite source for recycled zircon and phenocrysts in rhyodacite lava at Crater Lake, Oregon. Earth and Planetary Science Letters 233 (3-4), 277-293.

Bacon, C.R., Metz, J., 1984. Magmatic inclusions in rhyolites, contaminated basalts, and compositional zonation beneath the Coso volcanic field, California. Contributions to Mineralogy and Petrology 85 (4), 346-365.

Bachmann, O., Bergantz, G.W., 2004. On the origin of crystal-poor rhyolites: extracted from batholithic crystal mushes. Journal of Petrology 45 (8), 1565-1582.

Bachmann, O., Dungan, M.A., Lipman, P.W., 2002. The Fish Canyon magma body, San Juan volcanic field, Colorado; rejuvenation and eruption of an upper-crustal batholith. Journal of Petrology 43 (8), 1469-1503.

Bennet, V.C., DePaolo, D.J., 1987, Proterozoic crustal history of the western United States as determined by neodymium isotopic mapping. Geological Society of America Bulletin 99, 674-685.

Brown, S.J.A., Fletcher, I.R.,1999. SHRIMP U-Pb dating of the pre-eruption growth history of zircons from the 340 ka Whakamaru ignimbrite, NZ: Evidence for >250 k.y. magma residence times. Geology 27, 1035-1038.

Cates, N.L., Miller, J.S., Miller, C.F., Wooden, J.L., Ericksen, S., Means, M., 2003. Longevity of plutonic systems: SHRIMP evidence from Aztec Wash and Searchlight plutons, Nevada, Geological Society of America,2003 Cordilleran Section Annual Meeting, Abstracts with Programs 35 (4), 25-2.

Charlier, B.L.A., Wilson C.J.N., Lowenstern, J.B., Blake, S., Van Calsteren, P.W., Davidson, J.P., 2005. Magma generation at a large, hyperactive silicic volcano (Taupo, New Zealand) revealed by U-Th and U-Pb systematics in zircons. Journal of Petrology 46 (1), 3-32.

Chesner, C.A., Rose, W.I., Deino, A., Drake, R., Westgate, J.A., 1991. Eruptive history of Earth's largest Quaternary caldera (Toba, Indonesia) clarified. Geology 19 (3), 200-203.

Christiansen, R.L., 1984. Yellowstone magmatic evolution; its bearing on understanding large-volume explosive volcanism. National Acadamy Press, 85-95.

Coleman, D.S., Gray, W., Glazner, A.F., 2004. Rethinking the emplacement and evolution of zoned plutons: Geochronologic evidence for incremental assembly of the Tuolumne Intrusive Suite, California. Geology 32 (5), 433-436.

Cruden, A.R. Gocott, J., McCaffrey, K.J.W., David, D.D., 2005. Timescales of incremental pluton growth: theory and a field-based test. Geological Society of America, 2005 Annual Meeting, Abstracts and Programs 56 (9), 131.

Davies, Gareth R., Halliday, Alex N., Mahood, Gail A., Hall, Chris M., 1994. Isotopic constraints on the production rates, crystallisation histories and residence times of pre-caldera silicic magmas, Long Valley, California. Earth and Planetary Science Letters 125, (1-4), 17-37.

Eichelberger, J.C.; Chertkoff, D.G.; Dreher, S.T.; Nye, C.J., 2000. Magmas in collision; rethinking chemical zonation in silicic magmas. Geology 28 (7), 603-606.

Falkner, C.M., Miller, C.F., Wooden, J.L., Heizler, M.T., 1995. Petrogenesis and tectonic significance of the calc-alkaline, bimodal Aztec Wash pluton, Elorado Mountains, Colorado River extensional corridor. Journal of Geophysical Research 94, 7885-7898.

Faulds, J.E., Feuerbach, D.L., Reagan, M.K., Metcalf, R.V., Gans, P.B., Walker, J.D., 1995. The Mount Perkins block, northwestern Arizona: An exposed cross section of an evolving, preextensional to syextensional magmatic system. Journal of Geophysical Research 100 (B8), 15249-15266.

Faulds, J.E., Geissman, J.W., Shafiqullah. M., 1992. Implications of paleomagnetic data on Miocene extension near a major accommodation zone in the Basin and Range province, northwester Arizona and southern Nevada. Tectonics 11(2), 204-227.

Faulds, J.E., Feuerbach, D.L., Miller, C.F., Smith, E.I., 2001. Cenezoic evolution of the northern Colorado River Extensional Corridor, southern Nevada and northwest Arizona. Utah Geological Association Publication 30-American Association of Petroleum Geologists Publication GB78, 239-271.

Gans, P.B., Bohrson, W.A., 1998. Suppression of volcanism during rapid extension in the Basin and Range Province, United States. Nature 279, 66-68.

George, B.E., Miller, C.F., Walker, B.A., and Wooden, J.L., 2005. Newberry Mountains Dike Swarm, southern Nevada: final, extension-related pulse of the Spirit Mountain batholith. Eos. Trans. AGU, 86 (18), Jt. Assem. Suppl., Abstract V13A-01, JA511.

Glazner, A.F., Bartley, J.M., Coleman, D.S., Gray, W.M., Taylor, R.Z., 2004, Are plutons assembled over millions of years by amalgamation from small magma chambers? GSA Today 14 (4/5).

Grunder, A.L., Klemetti, E.W., 2005. Volcanic record of batholith assembly: the Aucanquilcha volcanic cluster, northern Chilean Andes. Geological Society of America, 2005 Annual Meeting, Abstracts and Programs 56 (7), 131.

Haapala, I., Ramo, O. T., Frindt, S., 2005, Comparison of Proterozoic and Phanerozoic rift-related basaltic-granitic magmatism. LITHOS 80 (1-4), 1-32.

Haapala, I., Ramo, O. T., Volborth, A., 1996, Petrogenesis of the Miocene granites of Newberry Mountains, Colorado River extensional corridor, southern Nevada, Geological Society of America, 1996 Annual Meeting, Abstracts with Programs, 28 (7), p. 420.

Haapala, I., Rämö, O.T., Volborth, A., 1995, Miocene rapakivi-like granites of southern Newberry Mountains, Nevada, U.S.A: Comparison to the Proterozoic rapakivi granites of Finland In: M. Brown and P.M. Niccoli (Eds.), The origin of granites and related rocks; Third Hutton Symposium, Abstracts, U.S. Geological Survey Circular 1129, 61–62.

Halliday, A.N., Mahood, G.A., Holden, P., Metz, J.M., Dempster, T.J., Davidson, J.P., 1989. Evidence for long residence times of rhyolite magma in the Long Valley magmatic system: the isotopic record in the precaldera lavas of Glass Mountain. Earth and Planetary Science Letters 94, 274-290.

Hawkins, D.P., Wiebe, R.A., 2003, High-precision temporal constraints on the construction of a periodically replenished, subvolcanic magma chamber: The Silurian Vinalhaven intrusion, Maine: The Origin of Granites and Related Rocks, Hutton Symposium V, abstracts, 91.

Hildreth, W., 2004, Volcanological perspectives on Long Valley, Mammoth Mountain and Mono Craters: several contiguous but discreet systems. Journal of Volcanology and Geothermal Research 136, 169-198.

Hildreth, W., 1981. Gradients in silicic magma chambers: Implications for lithospheric magmatism. Journal of Geophysical Research 86, 101153-10192.

Hopson, C.A., Gans, P.B., Baer, E., Blythe, A., Calvert, A., and Pinnow, J., 1994. Spirit Mountain Pluton, Southern Nevada: A Progress Report. Geological Society of America, 1994 Cordilleran Section, Abstracts with Programs, 60.

Howard, K.A., John, B.E., Davis, G.A., Anderson, J.L., Gans, P.B., 1994. A guide to Miocene extension and magmatism in the lower Colorado River Region, Nevada, Arizona, and California, A guide for Field Trip 3 Eighth International Conference on Geochronology, Cosmochronology, and Isotope Geology, May 31-June 4, 1994.

Howard, K.A., Wooden, J.L., Simpson, R.W., 1996. Extension-related plutonism along the Colorado River Extensional Corridor. Geological Society of America, 1996 Annual Meeting, Abstracts and Programs, A-450.

Hunt, C.B., Averitt, P., Miller, R.L. 1953. Geology and geography of the Henry Mountains region, Utah. USGS Professional Paper 228, 151

Iyer, H.M., Evans, J.R., Dawson, P.B., Stauber, D.A., Achauer, U., 1990. Differences in magma storage in different volcanic environments as revealed by seismic tomography; silicic volcanic centers and subduction-related volcanoes, In: Ryan, M.P. (Ed.), Magma transport and storage. United Kingdom, John Wiley & Sons, 293-316.

Koyaguchi, T., Kaneko, K., 2000. Thermal evolution of silicic magma chambers after basalt replenishments. Transactions of the Royal Society of Edinburgh: Earth Sciences 91 (1-2), 46-60.

Lee, Y.F.S.., Miller, C.F., Unkefer, J., Heizler, M.T., Wooden, J.L., and Miller, J.S., 1995. Petrology, emplacement, and tectonic setting of the Nelson pluton, Eldorado Mountains, Nevada. Eos. Trans. AGU 76 (17), S290.

Lees, J.M., 2005. Tomography of crustal magma bodies. Geological Society of America, 2005 Annual Meeting, Abstracts and Programs 56 (8), 131.

Lowery, L.E., Miller, C.F., Walker, B.A., Wooden, J.L., Mazdab, F.K., Bea, F., in press. Tracking magmatic processes in felsic magmas through Zr/Hf ratios in rocks and Hf and Ti zoning in zircons: an example from the Spirit Mountain batholith, Nevada. Mineralogical Magazine.

Ludwig, K.R., 2003. Isoplot 3.00: A geochronological toolkit for Microsoft Excel. Berkeley, CA: Berkeley Chronological Center.

Mahood, G.A., 1990. Second reply to comment of R.S.J. Sparks, H.E. Huppert and C.J.N. Wilson on “Evidence for long residence times of rhyolite magma in the Long Valley magmatic system: the isotopic record in the precaldera lavas of Glass Mountain”. Earth and Planetary Science Letters 99, 395-399.

McCaffrey, K.J.W., Petford, N., 1997. Are granitic intrusions scale invariant? Journal of the Geological Society 154 (1-4), part 1.

Metcalf, R.V., 2004. Volcanic-plutonic links, plutons as magma chambers and crust-mantle interaction: a lithospheric scale view of magma systems. Transactions of the Royal Society of Edinburgh-Earth Sciences 95 (1-2), 357-374.

Metcalf, R.V., Smith, E.I., Walker, J.D., Reed, R.C., Gonzales, D.A., 1995. Isotopic disequilibrium among commingled hybrid magmas; evidence for a two-stage magma mixing-commingling process in the Mt. Perkins pluton, Zrizona. Journal of Geology 103, 509-527.

Miller, C.F., Lowery, L.E., Bea, F., 2005. Zircon and Zr/Hf: assessing magmatic fractionation in the crust. 15th Annual Goldschmidt Abstract with Programs, A10.

Miller, C.F., McDowell, S.M., Mapes, R.W., 2003. Hot and cold granites? Implications of zircon saturation temperatures and preservation of inheritance. Geology 31 (6), 529-532.

Miller, C.F., Miller J.S., 2002. Contrasting stratified plutons exposed in tilt blocks, Eldorado Mountains, Colorado River Rift, Nevada, USA. LITHOS 61, 209-224.

Miller, C.F., Kapp, J.L., Ayers, J.C., Coath, C.D., Harrison, T.M., 1997. BSE imaging and ion probe geochronology of zircon and monazite from plutons of the Eldorado and Newberry Mountains, Nevada: age, inheritance, and subsolidus modification. *EOS*, 78, p.F783

Miller, JS, Miller, CF, Cates, NL, Wooden, J, Means, MA, Ericksen, S., 2004, Time scales of pulsatory magmatic construction and solidification in Miocene subvolcanic systems, Eldorado Mountains, Nevada (USA). Eos. Trans. AGU, 85, JA 496.

Miller, J.S., Wooden, J.L., 2004. Residence, Resorption and recycling of zircons in Devils Kitchen rhyolite, Coso Volcanic Field, California. Journal of Petrology 45 (11), 2155-2170.

Paterson, S.R., Miller, R.B., 1998. Mid-crustal magmatic sheets in the Cascades Mountains, Washington; implications for magma ascent. Journal of Structural Geology 20 (9-10), 1345-1363

Rämö, O.T., Haapala, I.J., Volborth, A., 1999. Isotopic and general geochemical constraints on the origin of Tertiary granitic plutonism in the Newberry Mountains, Colorado River Extensional Corridor, Nevada. Geological Society of American, 1999 Cordilleran Section, Abstracts with Programs 31 (6), p. A86.

Sambridge, M.S., Compston, W., 1994. Mixture modeling of multi-component data sets with application to ion-probe zircon ages. Earth and Planetary Science Letters 128, 373-390.

Schmitt, A.K., Lindsay, J.M., de Silva, S., Trumbull, R.B., 2002. U-Pb zircon chronostratigraphy of early-Pliocene ignimbrites from L Pacana, north Chile: implications for the formation of stratified magma chambers, Journal of Volcanology and Geothermal Research, 120, 43-53.

Simon, J.I., Reid, M.R., 2005. The pace of rhyolite differentiation and storage in an 'archetypical' silicic magma system, Long Valley, California. Earth and Planetary Science Letters 235, 123-140.

Steinwinder, T.R., Miller, C.F., Faulds, J.E., Koteas, G.C., Ericksen, S.M. 2004. Transition from plutonism to voluminous diking in the Eldorado mountains, northern Colorado River extensional corridor. Geological Society of America, 2004 Cordilleran Meeting, Abstracts with Programs 36(4), 8.

Vazquez, J.A., Reid, M.R., 2002. Time scales of magma storage and differentiation of voluminous high-silica rhyolites at Yellowstone caldera, Wyoming. Contributions to Mineralogy and Petrology 144, 274-285.

Volborth, A., 1973. Geology of the granite complex of the Eldorado, Newberry, and northern Dead Mountains, Clark County, Nevada. Nevada Bureau of Mines and Geology, Bulletin 80, 1-40.

Walker, B.A.., Miller, C.F., George, B.E., Luddington, S., Wooden, J.L., Bleick, H.A., Miller, J.S., 2005. The Spirit Mountain Batholith: Documenting Magma Storage in the Upper Crust one Pulse at a Time. Eos. Trans. AGU, 86 (18), Jt. Assem. Suppl., Abstract V21A-03, JA516.

Watson, E.B., Harrison, T.M., 1983. Zircon saturation revisited—temperature and composition effects in a variety of crustal magma types. Earth and Planetary Science Letters 64 (2), 295-304.

Watson, E.B., Harrison, T.M., 2005. Zircon thermometer reveals minimum melting conditions on earliest Earth. Science 308 (5723), 841-844.

Westerman, D.S., Dini, A., Innocenti, F., Rocchi, S., 2004, Rise and fall of a nested Christmas-tree laccolith complex, Elba Island, Italy. In: Breitkreuz, C. and Petford, N. (Eds.), Physical Geology of High-Level Magmatic Systems. Geological Society, London, Special Publication 234, 195-213.

Wiebe, Robert A., 1994. Silicic magma chambers as traps for basaltic magmas; the Cadillac Mountain intrusive complex, Mount Desert Island, Maine. Journal of Geology 102 (4), 423-437.

Wooden, J.L., Miller, D.M., 1990. Chronologic and isotopic framework for Early Proterozoic crustal evolution in the eastern Mojave Desert region, SE California. Journal of Geophysical Research 95, 20133-20146.